



UNIVERSIDAD DE CHILE
FACULTAD DE CIENCIAS FÍSICAS Y MATEMÁTICAS
DEPARTAMENTO DE INGENIERÍA CIVIL

**WHAT DOES THE STANDARDIZED STREAMFLOW INDEX
ACTUALLY REFLECT? SOME INSIGHTS FOR HYDROLOGICAL
DROUGHT ANALYSIS**

TESIS PARA OPTAR AL GRADO DE MAGÍSTER EN CIENCIAS DE LA INGENIERÍA,
MENCIÓN RECURSOS Y MEDIO AMBIENTE HÍDRICO

FABIÁN PATRICIO LEMA GONZÁLEZ

PROFESOR GUÍA:
PABLO MENDOZA ZÚÑIGA

MIEMBROS DE LA COMISIÓN:
MAURICIO ZAMBRANO-BIGIARINI
NICOLÁS VÁSQUEZ PLACENCIA
XIMENA VARGAS MESA

SANTIAGO DE CHILE
2024

RESUMEN DE LA TESIS PARA OPTAR AL

GRADO DE: Magíster en Ciencias de la Ingeniería,
mención Recursos y Medio Ambiente Hídrico

POR: Fabián Patricio Lema González

FECHA: 2024

PROFESOR GUIA: Pablo Mendoza Zúñiga

**¿QUÉ REFLEJA REALMENTE EL ÍNDICE ESTANDARIZADO DE CAUDALES?
ALGUNAS PERSPECTIVAS PARA EL ANÁLISIS DE SEQUÍAS HIDROLÓGICAS**

Las sequías hidrológicas son amenazas naturales que generan grandes impactos tanto para los ecosistemas naturales como para la sociedad. Para la detección y caracterización de este tipo de eventos es común el uso del índice estandarizado de caudal (SSI por sus siglas en inglés), debido a su sencilla formulación e interpretación. Las fluctuaciones en el índice SSI resumen la interacción entre distintos procesos hidrológicos, cuya desagregación presenta desafíos en la explicación de la respuesta hidrológica de una cuenca ante períodos de escasez hídrica. Además, su método de cálculo es particularmente sensible a la escala temporal utilizada, lo que impacta a la frecuencia y duración de los eventos de sequía hidrológica detectados y, en consecuencia, nuestra comprensión del fenómeno. En este estudio, se exploran las posibles relaciones entre el índice SSI y otras variables hidrológicas e índices estandarizados. Para ello, se implementa el modelo hidrológico SUMMA, acoplado al modelo de rastreo de escorrentía mizuRoute, en seis cuencas con diferentes regímenes hidrológicos ubicadas en Chile Central. Utilizando datos de precipitación extraídos del producto meteorológico CR2MET v.2.0 y los resultados del modelo a una escala mensual, se examinan las correlaciones entre el índice SSI y los principales flujos y almacenamientos simulados en cada cuenca (precipitación, humedad del suelo, equivalente de agua nieve y contenido de agua en el acuífero), considerando diferentes agregaciones temporales. Los resultados revelan diferencias entre los distintos regímenes hidrológicos, existiendo una alta dispersión en los valores de correlación de Spearman (hasta 0,5 de diferencia) entre distintas escalas temporales del índice SSI al evaluar períodos de agregación mayores a nueve meses en cuencas pluviales y mixtas, lo que no se evidenció en cuencas nivales. No obstante, en todas las cuencas estudiadas las mayores correlaciones (sobre 0,7) se encontraron al comparar el SSI de seis meses con variables hidrológicas agregadas a períodos de entre nueve y doce meses, con la sola excepción del almacenamiento del acuífero en cuencas nivales. Además, se analiza la trayectoria de propagación desde eventos de sequías meteorológicas hasta su manifestación como sequías de humedad del suelo e hidrológicas, considerando escalas temporales tradicionalmente usadas para el cálculo de índices estandarizados (uno, tres y doce meses). Se verifica que el uso de distintos criterios puede generar trayectorias drásticamente diferentes, e incluso contradictorias, para un mismo evento y una misma cuenca. Estos hallazgos refuerzan la importancia que posee el entendimiento de las relaciones entre los procesos hidrológicos en el cálculo de los índices estandarizados de sequía, por lo que se recomienda precaución al interpretar los resultados derivados de ellos, en especial al considerar cuencas que poseen diferentes regímenes hidrológicos.

Agradecimientos

Sacar adelante el magíster no hubiese sido posible sin el apoyo incondicional de mi familia en todo momento, sobre todo después de los difíciles momentos que nos ha tocado vivir estos últimos años. En especial gracias a mi papá y tía Pilar que han sido fundamentales en estos primeros años de vida independiente. Y gracias a mis hermanos, abuela, tíos y primos porque, a pesar de que hoy ya no nos reunamos tan seguido como antes, la comunicación nunca se ha perdido.

Agradezco todo el apoyo brindado por la comisión que participó de esta tesis. A la profesora Ximena y al profesor Mauricio por su dedicación y siempre buena voluntad al momento de plantear sugerencias, dudas y comentarios que sin duda enriquecieron muchísimo este trabajo. A Naoki por toda su ayuda durante la pasantía en Colorado. A Nicolás por tener siempre buena disposición a la hora de explicar, desde simples dudas sobre cómo cambiar el color de una imagen hasta cómo poder manejarme bien usando Leftraru. Y finalmente al profesor Pablo, por aceptar ser mi profesor guía y apoyarme desde el primer día durante este proceso, siempre con el mejor de los ánimos y energías.

A Gabi, Naro, Montse, Pablo, Nico y todos los compañeros de magíster con los que tuve la oportunidad de compartir este último par de años, ya presencial por suerte. Las largas horas de trabajo en la salita siempre fueron más llevaderas gracias a las conversaciones de almuerzo y tardes de juego de mesa.

A Jacqueline y al profe Yarko por su ayuda desde que entré al magíster, siempre con la mejor de las voluntades para resolver cualquier duda o problema que surgiera.

A Jorquera, Karen, Nico, Piccolis, Pincheira, Oliva, Jaja, Carlete y Oliva por su compañía desde los primeros años de universidad. A Daniel, Feli, Carlos y Jorge por mantener el contacto luego de tantos años. Gracias por su amistad, por compartir con ustedes muchos de mis mejores momentos y estar presentes también en los momentos difíciles.

Y finalmente gracias a todas las personas que, de alguna u otra forma, han formado parte de mi vida durante estos años.

Tabla de contenido

Capítulo 1: Introducción.....	1
1.1. Motivación	1
1.2. Objetivos	2
1.2.1. Objetivo General	2
1.2.2. Objetivos Específicos.....	3
Capítulo 2: Artículo para publicación.....	4
1. Introduction	5
2. Study area and data.....	7
2.1 Case study basins	7
2.2 Datasets	9
3. Approach	9
3.1 Hydrological modeling.....	10
3.2 Model calibration and evaluation.....	11
3.3 Drought analysis.....	11
4. Results	13
4.1 Hydrologic model performance	13
4.2 Impacts of temporal aggregation.....	14
4.3 Controls on SSI fluctuations	18
4.4 Effects of temporal aggregation on drought propagation.....	21
5. Discussion.....	23
5.1 Drought detection and characteristics	23
5.2 Drivers of the SSI across hydrological regimes	24
5.3 Limitations and future work	24
6. Conclusions	25
Acknowledgments	26
List of figures.....	27
List of tables.....	27
Capítulo 3: Conclusiones	28

Bibliografía.....	30
ANEXO.....	38

Capítulo 1: Introducción

1.1. Motivación

Las sequías son amenazas naturales recurrentes que pueden cubrir grandes extensiones territoriales y perdurar por períodos que van desde algunos meses hasta incluso décadas (Samaniego et al., 2013; Brunner & Tallaksen, 2019), generando un gran impacto tanto para los ecosistemas naturales como para las actividades socioeconómicas (Vicente-Serrano et al., 2020). Chile Central es una región que frecuentemente se ha visto afectada por este fenómeno, destacando eventos de sequías recientes como la del año 1998 y la denominada “mega-sequía” (Garreaud et al., 2017), originada en el año 2010 y que perduró en forma ininterrumpida hasta el año 2022 (Garreaud et al., 2019). Este último episodio provocó importantes alteraciones en múltiples componentes del ciclo hidrológico, incluyendo la precipitación, cobertura nival, almacenamiento en los acuíferos y caudal, generando déficits entre un 20 y 70% respecto a los valores normales previos (Garreaud et al., 2017). Además, generó impactos sobre el suministro de agua potable rural, y provocó cambios sobre el paisaje y vegetación de ecosistemas de la zona Centro-Norte de Chile (Garreaud et al., 2017).

Los eventos de sequía meteorológica tienen su origen en déficits de precipitación (McKee et al., 1993), los que a su vez pueden ser provocados por fluctuaciones relacionadas con la variabilidad interna del clima, como por ejemplo el fenómeno de El Niño Oscilación Sur (ENSO; Okumura et al., 2017). Sin embargo, las tendencias recientes, así como las proyecciones del calentamiento de la atmósfera – gracias a la contribución antropogénica al cambio climático (Hansen & Stone, 2016; Rosenzweig & Neofotis, 2013) – podrían afectar directamente a estos eventos (Boisier et al., 2015), incrementando su frecuencia, severidad y duración en múltiples regiones del planeta (Cook et al., 2014).

Existen varias definiciones de sequía, aunque todas tienen como base la noción de un período con los flujos y almacenamientos de agua por debajo de los valores promedio en una cuenca (Tallaksen & Van Lanen, 2004). Por otra parte, existen múltiples criterios para clasificar sequías, siendo los tipos más comunes la sequía meteorológica (precipitación), agronómica (humedad del suelo), hidrológica (caudal superficial y niveles de agua subterránea) y socioeconómica (Wilhite & Glantz, 1985). Entre ellos, es de especial relevancia la sequía hidrológica, debido a su impacto directo sobre ecosistemas naturales, el abastecimiento de agua potable, la agricultura y la industria; siendo su estudio una tarea fundamental para la planificación y gestión de los recursos hídricos (Zhang et al., 2022).

Para detectar y estudiar las características de los eventos de sequía, como por ejemplo su duración e intensidad, es común el uso de índices estandarizados como, por ejemplo, el Índice Estandarizado de Precipitación (SPI por sus siglas en inglés; McKee et al., 1993), el Índice Estandarizado de Precipitación-Evapotranspiración (SPEI por sus siglas en inglés; Vicente-Serrano et al., 2010; Beguería et al., 2014), el Índice Estandarizado de Caudales (SSI por sus siglas en inglés; Vicente-Serrano et al., 2012) y el Índice Estandarizado de Humedad del Suelo (SSMI por sus siglas en

inglés; Carrao et al., 2013). Si bien estos índices permiten comparar en forma directa sequías ocurridas en distintas regiones climáticas y geográficas, existe un conocimiento limitado sobre los procesos que realmente explican sus fluctuaciones. Adicionalmente, tampoco existe un consenso sobre la metodología más adecuada para su cálculo y, en particular, sobre cuál es la escala temporal más idónea a utilizar en cuencas que presentan diferentes climas o regímenes hidrológicos. La escala temporal hace referencia a una ventana de tiempo hacia atrás, normalmente medida en meses, sobre la cual se calcula un valor representativo (promedio o suma) de una variable hidrológica (precipitación, caudal, humedad del suelo, entre otras) y tiene efectos en la manera en que se interpreta el índice. Por ejemplo, una escala temporal mensual indica un solo valor del índice en cada mes, mientras que una trimestral, un valor representativo del índice cada tres meses.

Los índices estandarizados se calculan a partir de series de tiempo de observaciones o simulaciones de variables hidrológicas, tales como escorrentía y niveles de acuíferos (Shukla & Wood, 2008). Una de las principales ventajas que explica el amplio uso de este tipo de índice es la simpleza de su formulación, cálculo e interpretabilidad para identificar anomalías. Existen numerosos estudios que emplean estos índices para diferentes propósitos, destacando el monitoreo (Nuñez et al., 2014), pronóstico (Sutanto & Van Lanen, 2021) y el análisis de propagación de sequías (Barker et al., 2016).

Sin embargo, la aplicabilidad de índices estandarizados como el SPI y el SSI debe ser tomada con precaución, debido a que es sensible a aspectos tales como la calidad y cantidad de los datos, el período de referencia escogido, la escala temporal, la distribución de probabilidad y el método de estimación de parámetros utilizado en el cálculo (Tijdeman et al., 2020). La mayoría de los estudios de propagación de sequías busca establecer posibles relaciones entre “sets” de índices calculados a varias escalas temporales y el SSI, siendo un mes la agregación temporal más utilizada en el caso de la sequía hidrológica (e.g. Baez-Villanueva et al., 2024). Sin embargo, existen estudios que han utilizado agregaciones de tres meses (e.g. Nuñez et al, 2014), seis meses (e.g. Oertel et al., 2020) o incluso mayores (e.g. Barker et al., 2016).

La alta subjetividad en el cálculo e interpretación de los índices estandarizados es la principal motivación del presente trabajo de tesis, que busca contribuir a un mejor entendimiento del SSI y las implicancias que tiene su forma de estimarlo sobre la detección, caracterización y propagación de eventos de sequía.

1.2. Objetivos

1.2.1. Objetivo General:

El objetivo principal de este trabajo fue evaluar el efecto que genera la decisión de usar distintas escalas temporales sobre el cálculo del índice estandarizado de caudales (SSI) en seis cuencas de diferente régimen hidrológico de Chile Central.

1.2.2. Objetivos Específicos:

- Identificar los almacenamientos y flujos de agua que presentan una mayor relación con el índice estandarizado de caudal, calculado en distintas escalas temporales, en cuencas de diferente régimen hidrológico.
- Analizar cómo la elección de escalas temporales recomendadas en la literatura afecta a la propagación de un mismo evento de sequía en una cuenca determinada, evaluando su progresión en duración e intensidad, desde su origen en una sequía meteorológica hasta su manifestación en una sequía de humedad del suelo e hidrológica.

Capítulo 2: Artículo para publicación

A continuación, se presenta el artículo titulado “*What does the Standardized Streamflow Index actually reflect? Some insights for hydrological drought analysis*”, actualmente en preparación para ser enviado a la revista *Hydrology and Earth System Sciences*:

What does the Standardized Streamflow Index actually reflect? Some insights for hydrological drought analysis

Fabián Lema¹, Pablo A. Mendoza^{1,2}, Nicolás Vásquez¹, Naoki Mizukami³, Mauricio Zambrano-Bigiarini^{4,5} and Ximena Vargas¹

¹Department of Civil Engineering, Universidad de Chile, Santiago, Chile

²Advanced Mining Technology Center, Universidad de Chile, Santiago, Chile

³Research Applications Laboratory, National Center for Atmospheric Research, Boulder, Colorado, USA

⁴Department of Civil Engineering, Universidad de La Frontera, Temuco, Chile

⁵Center for Climate and Resilience Research, Universidad de Chile, Santiago, Chile

Abstract

Hydrological drought is one of the main hydroclimatic hazards worldwide, affecting water availability, ecosystems and socioeconomic activities. This phenomenon is commonly characterized by the Standardized Streamflow Index (SSI), which is widely used because of its straightforward formulation, calculation, and interpretability. Nevertheless, the applicability of the SSI is challenged by its sensitivity to the calculation method and, in particular, the choice of temporal scale, which can yield dramatic differences in drought detection and characterization. Moreover, there is limited understanding of what the SSI truly reveals about the underlying physical processes. To fill these gaps, we implemented the SUMMA hydrological model coupled with mizuRoute routing model in six case study basins located on the western slopes of extratropical Andes. Catchment-scale precipitation and model simulations were temporally aggregated to monthly time steps to examine correlations between the SSI and the main catchment-scale simulated fluxes and storages aggregated at different temporal scales. We found noteworthy differences in the relationships obtained among hydrological regimes. In particular, rainfall-dominated basins presented a higher dispersion in the correlation values achieved by temporal aggregations of SSI (1, 3 and 6 months) compared to snowmelt-driven basins, especially when we evaluated temporal scales longer than 9 months. In all the basins analyzed, the strongest relationships (Spearman correlation values over 0,7) were obtained when using 6-month aggregations to compute the SSI and 9-12 months to compute the explanatory variables, except aquifer storage in snowmelt-driven basins. Additionally, we unveiled the effects of adopting commonly used temporal scales on propagation analyses of specific drought events – from meteorological to soil moisture and hydrological drought – with a focus on their duration and intensity. The results reveal that the portrayal of drought propagation may change drastically, even in opposite directions for the same event, depending on this subjective decision.

1. Introduction

Droughts are natural hazards that can cover vast areas over a period of months to several years (Samaniego et al., 2013; Brunner & Tallaksen, 2019), with large effects on environmental systems (Vicente-Serrano et al., 2020) and socioeconomic activities (Wilhite & Pulwarty, 2017). These events are primarily triggered by precipitation deficits (McKee et al., 1993), which may be caused by the interplay of fluctuations associated to internal climate variability modes – such as El Niño Southern Oscillation (ENSO; e.g., Okumura et al., 2017; Steiger et al., 2021) – and exacerbated by land-atmosphere interactions (e.g., Schumacher et al., 2022). Given the warming trends projected for the next decades (e.g., Brunner et al., 2020; Tokarska et al., 2020) and the contribution of high temperature to drying (Trenberth et al., 2014), anthropogenic climate change is also expected to affect drought characteristics, increasing their frequency, severity, and duration in many regions of the world (e.g., Cook et al., 2014; Boisier et al., 2016; Pokhrel et al., 2021).

Despite the drought concept relies on the notion of below-average water fluxes and/or storages (Tallaksen & Van Lanen, 2004; Van Loon, 2015), there are several definitions and classifications, being meteorological (below-normal precipitation), soil moisture, hydrological (surface and groundwater level deficits) and socioeconomic the most commonly used types (Wilhite & Glantz, 1985). Among these, hydrological droughts – associated with abnormally low levels in groundwater, surface water bodies, and/or streamflow in rivers (Van Loon, 2015) – are especially relevant due to their direct impacts on natural ecosystems and human society. Hence, understanding how climate anomalies propagate through the terrestrial water cycle to trigger hydrological droughts of different characteristics (e.g., duration, severity) is an ongoing challenge for the scientific community, and a crucial task for water resources planning and management (Zhang et al., 2022).

Hydrological droughts are typically characterized through indices derived from observed or modeled time series of groundwater levels (e.g., Bachmair et al., 2015), runoff (e.g., Shukla & Wood, 2008), and streamflow (e.g., Zhu et al., 2016; Stahl et al., 2020). Among the existing indices, the Standardized Streamflow Index (SSI; Vicente-Serrano et al., 2012) has become increasingly popular because of its straightforward formulation, calculation, and interpretability for the characterization of discharge anomalies. In fact, a search in the Clarivate Analytics Web of Science platform using the keywords “standardized streamflow index” (or “standardised streamflow index”) and “drought” revealed 122 journal articles at the time of this writing, being 62 published during the period 2021-2023. Such body of work spans various areas, including drought monitoring (e.g., Núñez et al., 2014; Nkiaka et al., 2017) and forecasting (e.g., Sutanto & Van Lanen, 2021; Sutanto & Van Lanen, 2022; Hameed et al., 2023), as well as drought propagation under historically observed (e.g., Barker et al., 2016; Bhardwaj et al., 2020) and projected (e.g., Wan et al., 2018; Adeyeri et al., 2023) climatic conditions.

The applicability of the SSI is challenged by its sensitivity to the quantity and quality of the data (Wu et al., 2018) and the calculation method, which entails the choice of a reference period for standardization, the selection of probability distribution (e.g., Teutschbein et al., 2022; Laimighofer & Laaha, 2022), the parameter estimation approach (e.g., Tijdeman et al., 2020) and, in particular,

the temporal scale (e.g., Barker et al., 2016; Svensson et al., 2017; Baez-Villanueva et al., 2023). The latter refers to the backward-looking period (commonly a number of months) over which streamflow values are averaged before computing the index. Most drought propagation analyses seek possible relationships between other standardized indices (e.g., McKee et al., 1993; Vicente-Serrano et al., 2010) computed for various temporal scales and the SSI for some another equal or different temporal scale, with one month (SSI-1) the most common choice (e.g., Huang et al., 2017; Peña-Gallardo et al., 2019; Stahl et al., 2020; Wang et al., 2020; Wu et al., 2022; Zhang et al., 2022; Baez-Villanueva et al., 2023; Odongo et al., 2023). Such decision commonly relies on the assumption that a one-month scale is representative of actual streamflow conditions that integrate time lags in other variables (e.g., Tijdeman et al., 2020; Sutanto & Van Lanen, 2021), enabling direct comparisons with them (e.g., Baez-Villanueva et al., 2023). Because the SSI-1 may be susceptible to short-term fluctuations, other authors have preferred smoothed (e.g., 3-month averages) time series of SSI-1 (e.g., Bhardwaj et al., 2020), 3-month (e.g., Núñez et al., 2014; Wu et al., 2017; Rivera et al., 2021; Adeyeri et al., 2023; Yun et al., 2023), 6-month (e.g., Seibert et al., 2017; Oertel et al., 2020), and even longer (e.g., Barker et al., 2016; Teutschbein et al., 2022; Fowé et al., 2023) temporal scales.

Nowadays, there is no consensus regarding the suitable temporal scale for both SSI and hydrological explanatory variables, which may stem from the limited understanding of what the SSI truly reveals about the underlying physical mechanisms driving hydrological droughts. For example, Buitink et al. (2021) examined five components of the water cycle – precipitation, soil moisture, vegetation greenness, groundwater and surface water – in the Dutch province of Gelderland, finding that percentile-based thresholds that are commonly used for hydrological drought detection mask out more frequent drought conditions that other variables in the system may be experiencing.

To tackle this issue, process-based hydrological modeling arises as a useful approach (Peters-Lidard et al., 2021), and the literature is rich in studies using models with varying degrees of complexity to analyze the propagation from meteorological to soil moisture or hydrological droughts (e.g., Andreidis et al., 2005; Sheffield & Wood, 2007; Van Loon & Van Lanen, 2012; Samaniego et al., 2013; Van Loon et al., 2014; Zink et al., 2016; Apurv et al., 2017; Bhardwaj et al., 2020; Lee et al., 2022; Rakovec et al., 2022). This paper contributes to this field by combining observed data and a state-of-the-art physics-based modeling framework to examine possible drivers that explain fluctuations in the widely used SSI across hydrological regimes. Here, we depart from previous assessments by first conducting exploratory analysis with modeled catchment-scale water storages and the SSI, to subsequently inform the choice of aggregation period for the calculation of standardized indices (e.g., Samaniego et al., 2013) commonly used in drought propagation analyses. Specifically, we address the following research questions:

1. What are the effects of different temporal scales on the number and duration of hydrological droughts?
2. How does the SSI relate to other water storages and fluxes across different hydrological regimes?

3. How do different temporal scales affect the propagation of historically observed meteorological droughts towards soil moisture and hydrological droughts?

To seek for answers, we configure the Structure for Unifying Multiple Modeling Alternatives (SUMMA; Clark et al., 2015a, 2015b) hydrological model and the vector-based routing model mizuRoute (Mizukami et al., 2016, 2021) in six case study basins located along the western slopes of the extratropical Chilean Andes. Catchment-scale precipitation and model simulations are temporally aggregated to monthly time steps to compute snow water equivalent (SWE), soil moisture, aquifer storage, total storage (i.e., the sum of SWE, soil moisture, aquifer storage, and canopy storage) and the SSI for different temporal scales. We use these time series to explore the physical processes explaining variations in the SSI during the period April/1983-March/2020, as well as the drought event of 1998/99 and the recent central Chile megadrought (Garreaud et al., 2017; Garreaud et al., 2019). Finally, we examine the implications for the calculation of commonly used indices in the portrayal of drought propagation of historically observed events. Our main goal is to improve the current understanding of the information content of the SSI across different hydrological regimes and raise awareness on the impact that the subjective choice of the temporal scale and the analysis periods may have on the interpretation and application of the SSI for drought monitoring and propagation analyses.

2. Study area and data

2.1 Case study basins

We conduct our analyses in six basins located on the western slopes of the extratropical Andes Cordillera in central Chile (Figure 1): (i) Cochiguaz River at El Peñón, (ii) Choapa River at Cuncumén, (iii) Claro River at El Valle, (iv) Palos River at Colorado, (v) Ñuble River at La Punilla, and (vi) Cautín River at Rari-Ruca. Hereafter, to identify each basin we use the name of the river. The catchment boundaries and the identification number (ID) are obtained from the CAMELS-CL database (Alvarez-Garreton et al., 2018). The basins span a wide range of physiographic characteristics and climatic conditions, with annual precipitation amounts ranging from 260 to 2900 mm/year, mean annual temperatures between 9 to 16 °C, annual runoff spanning 114-2090 mm/year and aridity indices between 0.4 to 3 (Table 1). Such climatic diversity translates into different hydrological regimes: the Cochiguaz and Choapa River basins are snow-driven, Palos and Ñuble have a mixed regime, while Claro and Cautín are mostly rainfall-driven. All basins have a snow component -except Cautín-, with an increase in discharge due to snowmelt between September and December (Spring) and receive most of the precipitation during the Fall (MAM) and Winter (JJA) seasons (Figure 1).

Table 1: Physiographic and climatic attributes of the six basins considered in this study. All data came from the CAMELS-CL database, except for the baseflow index, which was estimated from hydrological simulations in the SUMMA model. The aridity index was calculated as PET/P.

Catchment	ID	Lat. (°)	Long. (°)	Elevation range (m)	Area (km ²)	Mean annual P (mm/yr)	Mean annual Q (mm/yr)	Runoff ratio (-)	Aridity index (-)	Baseflow index (-)
Cochiguaz	4313001	-30.30	-70.28	1341-5275	675	259	114	0.44	3.8	0.99
Choapa	4703002	-32.10	-70.45	1153-5038	1132	392	231	0.59	2.3	0.98
Claro	6027001	-34.85	-70.73	542-3046	349	1414	891	0.63	0.7	0.42
Palos	7115001	-35.44	-70.74	590-3282	490	1960	1686	0.86	0.5	0.81
Ñuble	8105001	-36.68	-71.19	645-3189	1254	2108	1792	0.82	0.5	0.71
Cautín	9123001	-38.47	-71.75	413-3090	1306	2906	2092	0.72	0.4	0.72

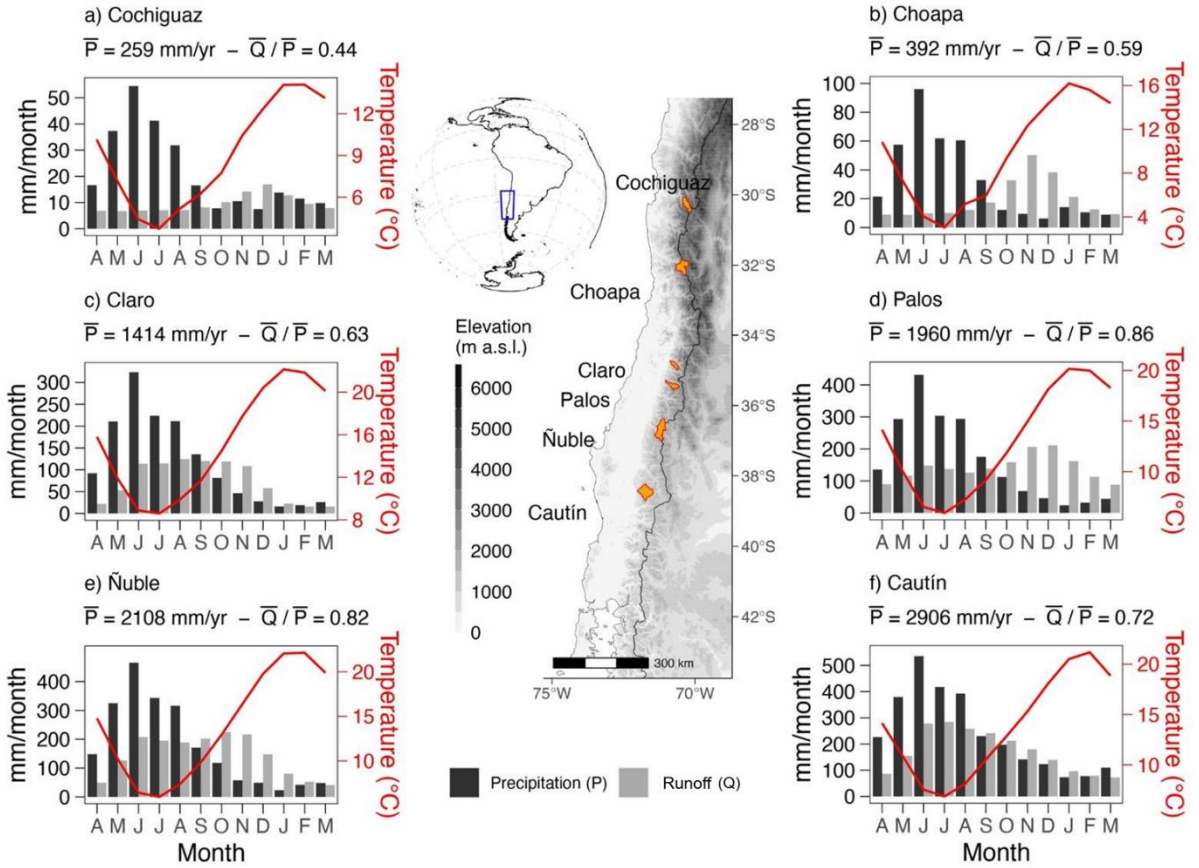


Figure 1: Location and seasonal variability of precipitation (P), runoff (Q) and temperature for the six case study basins: (a) Cochiguaz River at El Peñón, (b) Choapa River at Cuncumén, (c) Claro River at El Valle, (d) Palos River at Colorado, (e) Ñuble River at La Punilla, and (f) Cautín River at Rari-Ruca. Overlines represent annual averages for the period April/1985-March/2015.

2.2 Datasets

Meteorological daily data are obtained from the CR2MET v.2.0 observational product (DGA, 2017; Boisier et al., 2018), which provides estimations of precipitation and extreme temperatures for the period 1979-2020 at a $0.05^\circ \times 0.05^\circ$ horizontal resolution. The daily precipitation estimations of this product are obtained using multiple linear regression models that consider variables from the fifth generation of the European Reanalysis (ERA5-Land; Muñoz-Sabater et al., 2021) and physiographic attributes as predictors. All variables derived from ERA5-Land are statistically downscaled to match the CR2MET horizontal resolution. For extreme daily temperatures, land surface temperature from the Moderate Resolution Imaging Spectroradiometer (MODIS) is included as a potential explanatory variable. Wind, incoming shortwave radiation, atmospheric pressure, and relative humidity are obtained from ERA5-Land, whereas incoming longwave radiation is computed using the formulation proposed by Iziomon et al. (2003). Land cover data and vegetation types for the study area are also obtained from MODIS. Daily streamflow records are collected by the Chilean Water Directorate (DGA) and were retrieved from the website of the Climate and Resilience Research Centre (CR2, <https://www.cr2.cl/datos-de-caudales/>).

3. Approach

Our approach considers the configuration of the SUMMA hydrological model and the mizuRoute routing model (Figure 2a); the calibration and evaluation of the SUMMA model parameters (Figure 2b); the computation of meteorological, agricultural and streamflow standardized drought indices derived from precipitation, simulated soil moisture and simulated streamflow, respectively (Figure 2c), as well as the analysis of their interplay with other simulated hydrological variables (Figure 2d). Finally, we examine how temporal aggregations typically adopted for the calculation of standardized indices affect the portrayal of historically observed drought events (Figure 2e). In the following subsections, we describe these steps in detail.

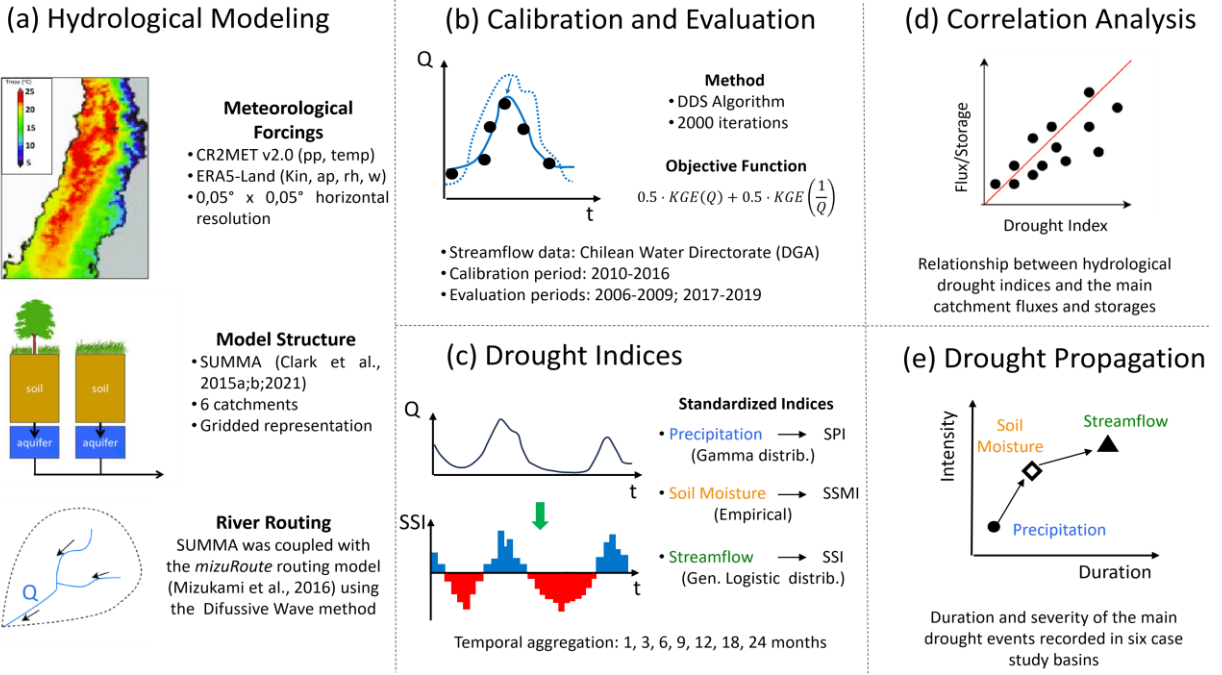


Figure 2: Flowchart describing the approach used in this study. See text for details.

3.1 Hydrological modeling

We use the SUMMA hydrologic modeling system, which offers different implementations for a wide range of modeling decisions. Specifically, SUMMA has several options for model configuration, process representations, and flux parameterizations for mass and energy balance equations. Here, we used the Jarvis (1976) function for simulating stomatal resistance, one of the main physiological factors controlling transpiration, similar to the Noah-MP land surface model (Niu et al., 2011). We also considered a logarithmic wind profile below the vegetation canopy - which parametrization is described in Mahat et al. (2013)- and implemented the Raupach (1994) parametrization for vegetation roughness length and displacement height. For the radiation transmission through vegetation parametrization, we use Beer's Law (Mahat and Tarboton, 2012), as is implemented in VIC model (Liang et al., 1994). For the vertical redistribution of water among soil layers, we considered the mixed form of the Richards equation (Celia et al., 1990), a constant hydraulic conductivity with depth and a lumped aquifer model. For snow, we consider a constant decay rate of albedo, while the thermal conductivity was parametrized using Jordan (1991) approach.

In this study, each basin is spatially discretized into a set of hydrologic response units (HRUs), arranged in a grid, with horizontal dimensions equal to the CR2MET observational dataset (i.e. 0,05° x 0,05°). Each HRU has specific physiographic characteristics (e.g., slope, elevation, layer thickness, vegetation, and soil type), a maximum of five snow layers, and three soil layers with different thicknesses -top: 0,5 m, middle: 2 m, down: 2,5 m -. Further, each HRU incorporates an unconfined aquifer at the bottom of the soil column, which contributes to baseflow generation (Figure 2a). We stress that each HRU is independent. Thus, no lateral water flow between HRUs is allowed.

Additionally, we use the vector-based routing model mizuRoute (Mizukami et al., 2016) to convert the instantaneous runoff obtained with the SUMMA model at each HRU into streamflow at the basin outlet. The application of mizuRoute requires the delineation of a digital river network, with individual subcatchments contributing runoff to each river reach. First, the model converts the total runoff from each HRU (i.e., grid cell) into sub catchment-scale runoff using area-weighted averages. Then, the model performs a hillslope routing to delay instantaneous total runoff from the sub-catchment to the corresponding outlet using a gamma-distribution-based unit hydrograph and then routes the delayed runoff for each river reach in the order defined by the river network topology. Full descriptions of the hillslope routing, general routing procedures, and routing schemes are provided by Mizukami et al. (2016). Here, we use the Diffusive Wave routing scheme described and implemented by Cortés-Salazar et al. (2023).

3.2 Model calibration and evaluation

We calibrated 14 parameters (Table S.1 in Supplementary material) of the SUMMA model using the Dynamically Dimension Search algorithm (DDS; Tolson & Shoemaker, 2007) implemented in the OSTRICH software (Matott, 2017), with a maximum number of 2000 iterations in each trial. We maximize the objective function (OF) proposed by Garcia et al (2017), which is focused on low-flow simulations of rainfall-runoff models (Eq 3.1).

$$OF = 0.5 \cdot KGE(Q) + 0.5 \cdot KGE(1/Q) \quad (3.1)$$

where KGE is the Kling-Gupta efficiency (Gupta et al., 2009). The data is split into a calibration period (April/2010 – March/2017) and two non-consecutive evaluation periods, totaling seven water years (April/2006 – March/2010 and April/2017 – March/2020). For model evaluation, we use the OF, KGE, Nash-Sutcliffe efficiency (NSE; Nash & Sutcliffe, 1970), coefficient of determination (R^2), and root mean square error (RMSE, Figure 2b).

3.3 Drought analysis

3.3.1 Drought Indices

For meteorological drought characterization, we use the Standardized Precipitation Index (SPI; McKee et al., 1993). The SPI compares the cumulative precipitation for a specific temporal scale with its long-term (usually 30 years or more) distribution at a given location. The SPI calculation involves (i) selecting a probability density function (PDF) and its parameters to obtain the reference long-term distribution for cumulative precipitation; (ii) obtaining the cumulative distribution function (CDF) from the fitted distribution; and (iii) transforming the CDF into a standardized normal distribution (i.e. with mean equal to zero and standard deviations of one), using an equipercentile inverse transformation to derive the SPI values. Here, we use the Gamma distribution and the probability-weighted moments method to estimate the parameters in SPI calculations. We also use the Standardized Precipitation and Evapotranspiration Index (SPEI; Vicente-Serrano et al., 2010), which is based on the simple and multitemporal nature of the SPI formulation. The calculation of the SPEI requires monthly precipitation and temperature data, and involves a mass balance given by precipitation minus potential evapotranspiration ($P-PET$), with the latter usually estimated by the Thornthwaite equation (Thornthwaite, 1948).

For soil moisture drought analysis, we use the Standardized Soil Moisture Index (SSMI; Carrao et al., 2013), which quantifies deficits in the soil water content in the root zone relative to its seasonal climatology at a specific location. The SSMI uses a non-parametric approach to fit monthly soil moisture series. Since the SUMMA model provides information of other storages besides soil moisture, we also propose and use a modified version – the Standardized Water Storage Index (SWSI) – to assess total water storage deficits, including SWE, canopy storage, soil moisture, and aquifer storage.

Finally, we use the Standardized Streamflow Index (SSI; Vicente-Serrano et al., 2010) for hydrological drought characterization. Despite a monthly scale being the most common choice (SSI-1; e.g., Stahl et al., 2020; Baez-Villanueva et al., 2023), several studies have used longer temporal scales, as long as 24 or 36 months (e.g., Barker et al., 2016). Here, we use the generalized logistic distribution to compute the index, following recommendations from past studies (e.g., Vicente-Serrano et al., 2010; Tijdeman et al., 2020).

We compute all the standardized drought indices (SDI) for multiple temporal scales (SDI-n, with $n = 1, 3, 6, 9, 12, 18$, and 24 months, Figure 2c). To define a drought event, we use two approaches: (i) fixed threshold method (Van Loon, 2015) with a value of -1 , which means that a drought condition is detected when monthly index values are below this specified threshold, and (ii) a more restrictive criteria based on $SDA-n < 1$ — as in the first approach — for at least a required minimum duration (e.g., Zhu et al., 2016). Here, we consider a minimum duration requirement of three consecutive months. We test these two approaches to evaluate how different degrees of drought definition may affect our results.

3.3.2 Correlation analysis

To understand the main drivers of temporal variations in the SSI, we compute the Spearman's rank correlation coefficient between SSI-n – with $n = 1, 3$, and 6 months, which are the most commonly used temporal scales in drought propagation analyses (e.g., Nuñez et al., 2014; Oertel et al., 2020) – and the main catchment-scale water fluxes and storages as explanatory variables (Figure 2d), including precipitation, snow water equivalent (SWE), soil moisture, aquifer storage and the total amount of storages within the basin (SWE, canopy storage, soil moisture and aquifer storage). We also consider different accumulation periods (with $n = 1, 3, 6, 9, 12, 18$, and 24 months) for each hydrological variable, using the temporal averages or additions over the preceding n-months, including the target month, to evaluate if different variables affect the SSI in a delayed period.

The correlation analyses were conducted independently at each case study basin over different historical temporal windows that span exceptionally dry water years – associated with meteorological drought –. The goal is to identify the strongest relationships between the SSI and explanatory variables, the associated temporal scales, and whether these vary substantially with hydrological regimes and/or drought episodes.

3.3.3 Drought propagation analysis

We used the time scales that maximized the linear correlation – identified in the previous step (section 3.3.2) – and the SPI, SSMI, and SSI indices to describe the transition from meteorological to hydrological droughts, passing through soil moisture droughts (SPI → SSMI → SSI; Figure

2e). In this analysis, we consider the duration (in months) and the intensity, measured as the temporally-averaged value obtained by the index during its respective drought period. We also compared the drought portrayals obtained with the temporal scales identified here, against other criteria adopted in recent studies, which involve analysis of temporal scales of 1-month (e.g. Leng, 2015; Bhardwaj, 2020), 3-months (e.g. Fuentes, 2022; Adeyeri, 2023), and of variable duration depending on the hydrological regime of the basin (Baez-Villanueva et al., 2023).

4. Results

4.1 Hydrologic model performance

Figure 3 displays hydrologic model calibration and evaluation results for the six study-case basins. The value of the objective function (Eq 3.1) during the evaluation period is higher than 0.73 in all basins (Figure 3a). The minimum KGE during the calibration period is 0.74 (Choapa), whereas the highest KGE values were achieved in the rainfall-driven catchments, being 0.83 and 0.82 at the Palos and Cautín River basins, respectively. Negative biases (i.e., underestimation of runoff volumes) are obtained for Cochiguaz (-15,4%) and Ñuble (-5,8%), while small (i.e., < 8%) positive biases are obtained in the remaining basins. In general, the observed daily flow duration curves are accurately by the SUMMA model in all catchments (Figure 3b). Similarly, the midsegment slope of the flow duration curve (20% - 70% flow exceedance probabilities) is adequately replicated, although there is an overestimation of low flow volumes with exceedance probabilities larger than 90% in the Choapa and Claro catchments (< 2 m³/s). The streamflow seasonality is well reproduced by the SUMMA model in all basins (Figure 3c), although there is an overestimation (< 10%) of mean monthly flows during September-November (i.e., when snowmelt occurs) at the Choapa and Claro River basins, and during March-October (i.e., when rainfall events occur) at the Ñuble and Cautín River basins.

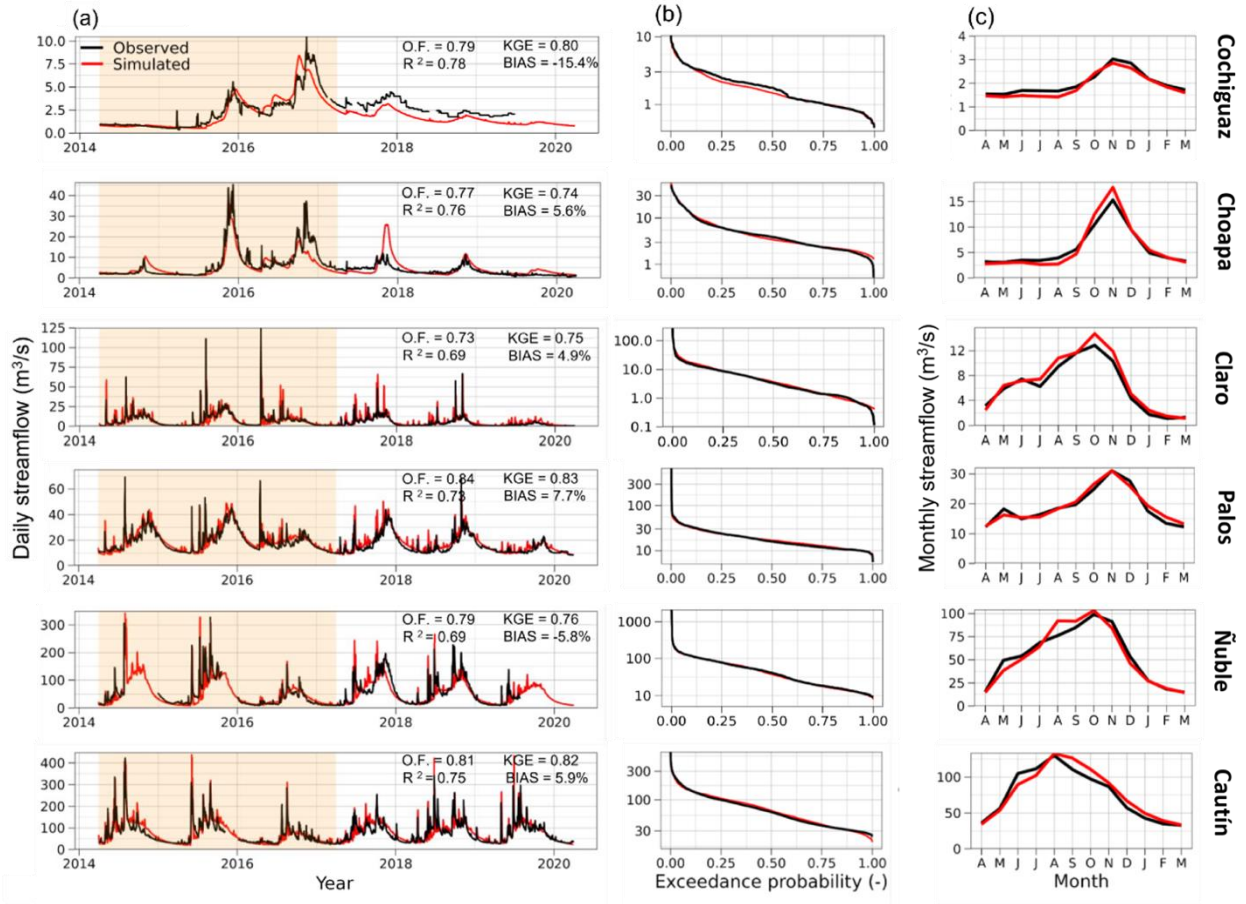


Figure 3. Comparison between simulated and observed streamflow for all basins in terms of (a) daily time series (April/2014 to March/2020), (b) daily flow duration curves (vertical logarithmic scale), and (c) mean monthly runoff. In (a) the shaded area represents part of the calibration (yellow) and evaluation (white) periods, and OF indicates the value of the objective function (Eq 3.1) over the evaluation period. The results in (b) and (c) correspond to the evaluation periods (April/2006 – March/2010 and April/2017 – March/2020) combined.

4.2 Impacts of temporal aggregation

Figure 4 illustrates the time series for different simulated variables, as well as the SPI and SSI indices computed at different temporal scales for the Choapa and Cautín River basins. We focus on a three-year period (1998-2000) that includes the year 1998, a remarkably dry year spanning a 6-month period (July-December) with abnormally low precipitation amounts. Such precipitation deficit had a noticeable impact on snow accumulation, especially in the Choapa River basin (snowmelt-driven), and affected other variables to a lesser degree, including soil moisture (agricultural drought) and aquifer storage, whose levels were even lower than those recorded in subsequent years. Ultimately, the meteorological drought translated into lower streamflow rates over the course of 1998 and even 1999.

Figures 4b and 4g show evident discrepancies among the SSI and SPI values obtained from different temporal scales – particularly in the SPI index – which are exacerbated when moving from aggregations larger than 12 months (18 and 24 months). This is especially noticeable in the

SSI time series of the Choapa River basin, where a similar behavior over time is observed for SSI-1, SSI-3, SSI-6, and SSI-9, with index values lower than -1 between October/1998 and September/1999. Conversely, the onset of hydrological drought was detected in May/1999 with SSI-18, and towards the end of 1999 when using SSI-24. Notably, the results in Figure 4g demonstrate that even a 1-month scale for SSI calculations can distort the actual variability of streamflow-records considerably.

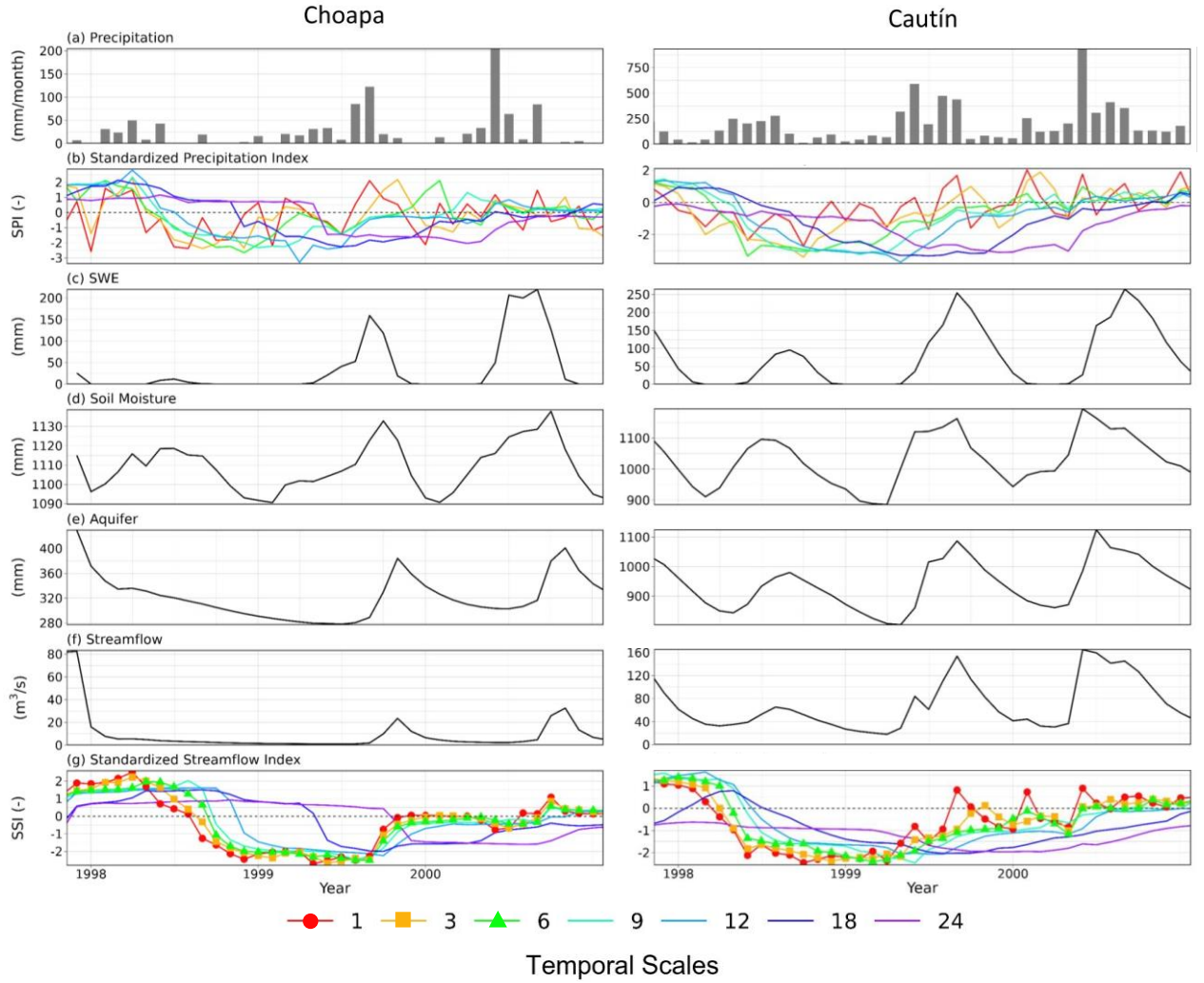


Figure 4: Monthly time series of (a) precipitation, (b) SPI, (c) SWE, (d) total soil moisture, (e) aquifer storage, (f) streamflow, and (g) SSI for the Choapa (snowmelt-driven, left) and Cautín (rainfall-driven, right) River basins. Monthly precipitation and SPI-n are obtained from the CR2MET meteorological product, whereas the remaining variables are obtained from SUMMA model simulations during January/1998–December/2000. Temporal aggregations of 1, 3 and 6 months for the SSI are highlighted due to their widespread use (see text for details).

The choice of temporal scales used to compute the SSI can also affect the estimated frequency and duration of hydrological drought events. This is illustrated in Figure 5, which compares the number of events detected with SSI-1, SSI-3, and SSI-6, as well as their duration over the entire simulation period (April/1983 – March/2020). The results displayed are classified according to two criteria: all detected drought events regardless of their duration – one-month duration events (“free”) –, and establishing as a requirement that detected drought events must have a minimum duration of at least three consecutive months (“constrained”). Figure 5a shows substantial differences in the number of events depending on the criteria and temporal scale used, with the only exception being the Cochiguaz River basin. In general, the number of events detected with the free criteria decreases for longer temporal aggregations, as opposed to the constrained criteria, for which such number tends to remain constant or even increase (see, for example, the Choapa River basin). The largest discrepancies are found in the rainfall-dominated catchments; for example, 28 and 13 events were detected with the SSI-1 and SSI-6, respectively, using the free criteria. Figures 5b and 5c display the empirical probability density functions of drought durations obtained with the free and constrained criteria for all basins and temporal scales, and Table 2 includes the average durations considering all the events during the analysis period. As for the frequency, we found no changes in the Cochiguaz River basin; however, the effects of temporal scales on drought durations are considerable in rainfall-driven catchments – especially with the free criteria –, with a transition from positively skewed density functions with averages between 1-3 months when using SSI-1, to more homogeneous distributions –centered around 8 months- when using SSI-6.

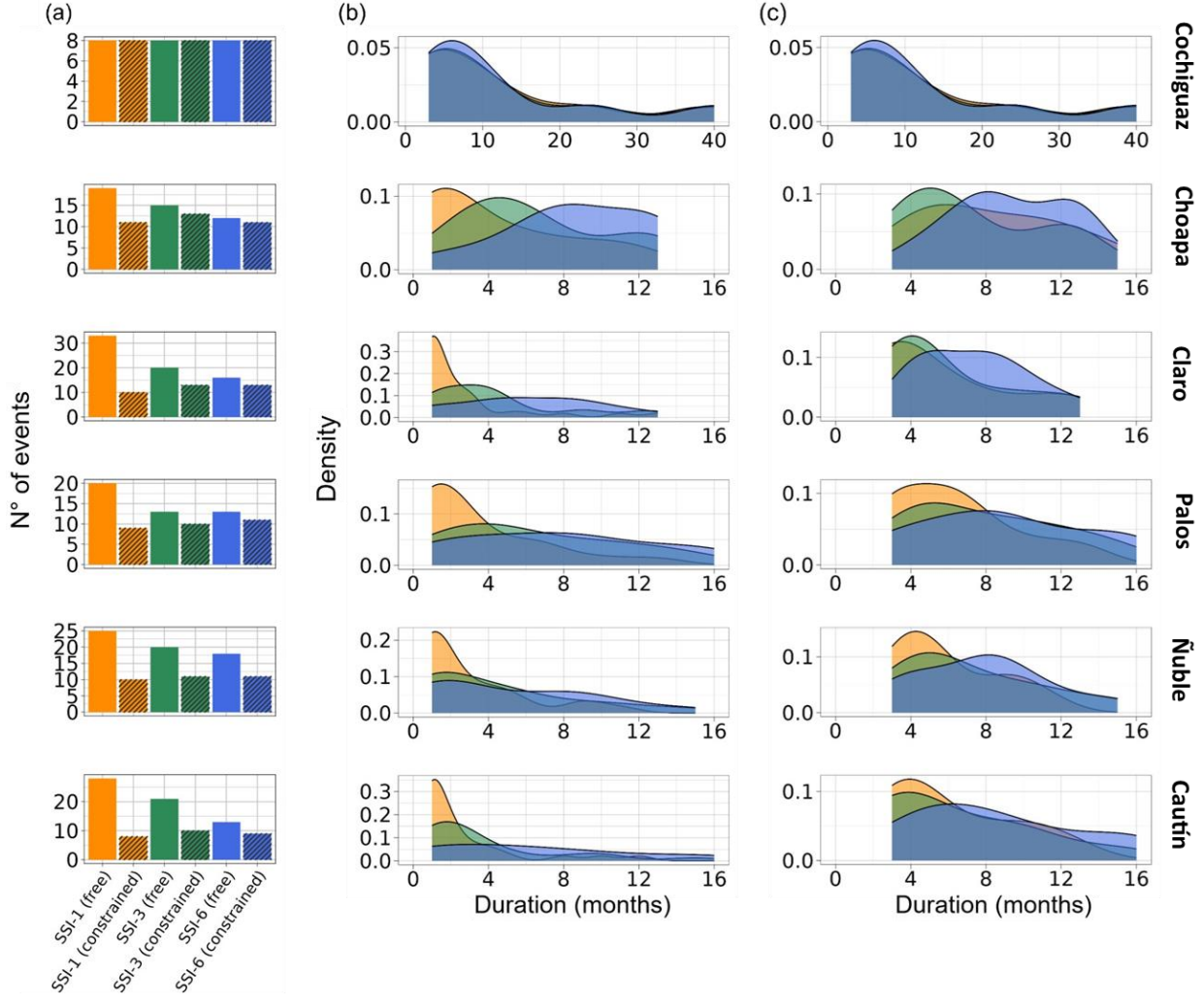


Figure 5: Effects of the choice of temporal scale (1, 3, and 6 months) in SSI calculations and duration restrictions on (a) the frequency and (b,c) duration of hydrological droughts detected between the water years 1983/84-2019/20. Probability distributions of drought durations are displayed for the cases (b) no restrictions (i.e., “free”), and (c) minimum drought duration of three months (i.e., “constrained”) for event detection (see text for details).

Table 2: Mean duration (in months) of drought events for each case and temporal scale of SSI.

Basin	Case 1: free			Case 2: constrained		
	SSI-1	SSI-3	SSI-6	SSI-1	SSI-3	SSI-6
Cochiguaz	12.25	12.50	12.88	12.25	12.50	12.88
Choapa	4.58	6.60	8.67	8.27	7.39	9.36
Claro	2.58	4.50	6.20	5.80	6.15	7.39
Palos	3.50	6.46	7.77	6.33	8.00	9.00
Ñuble	3.04	4.50	5.28	5.90	7.27	7.91
Cautín	2.64	3.81	6.31	6.13	6.50	8.67

4.3 Controls on SSI fluctuations

Figure 6 illustrates the impacts of the temporal scale used to compute the SSI on the relationships between the precipitation and catchment storages obtained for different aggregation periods. Note that when computing the correlation, the variables are contrasted considering different temporal scales of SSI. One can note that the differences are minimal between the SSI-1, SSI-3, and SSI-6 for the two snowmelt-driven basins (i.e., Cochiguaz and Choapa). Further, the shape of the curves is similar in most cases, achieving the highest correlations with precipitation and SWE on a 12-month scale, and the highest correlations with soil moisture and total storage using temporal scales between 6 and 12 months. Notably, possible dependencies between the SSI and aquifer storage vary depending on the hydrological regime. In fact, the relationship is stronger for smaller temporal scales (i.e., 3-6 months) of aquifer storage in snowmelt-driven basins, whereas correlation is maximized for scales of 9-12 months in rainfall-dominated catchments.

In most cases, the highest (lowest) correlations are obtained using SSI-6 (SSI-1), although there are some exceptions for temporal scales shorter than 9 months at the Palos and Ñuble River basins (mixed regime), where higher correlations are achieved when using SSI-1. The impacts of the temporal scale on correlation results are considerably larger in basins with mixed or rainfall-dominated regimes, where there is larger dispersion in the correlation achieved by the indices, reaching differences up to 0.5 in the Ñuble and Cautín River basins for a 12-month scale. Similarly, a progressive increase in the dispersion of correlations is observed when evaluating indices at larger temporal scales (> 9 months) for all storages in mixed and rainfall-driven catchments.

Figure 7 displays correlations between the SSI-6 and the hydrological variables -aggregated at different temporal scales- for the six case study basins and three periods: the 1998/1999 drought event, the central Chile megadrought (2010-2019), and the entire period of analysis (April/1983 - March/2020). The same analysis was also performed for SSI-1 and SSI-3, which are shown in Figures S.1 and S.2 in the Supplementary material. The examination of different storages reveals that, in general, higher (lower) correlations are obtained in arid and snowmelt-driven (humid and rainfall-driven) basins, regardless of the temporal scale analyzed. In other words, there are stronger relationships with SSI-6 in the northern regions (aridity index > 2 and mean annual P < 400 mm/yr), which gradually become weaker towards the south (aridity index < 0.5 and mean annual P > 2000 mm/yr), following the central Chile's hydroclimatic gradient. Such pattern is more evident when all catchment storages are aggregated (last row in Figure 7) and to a smaller degree in individual storages (SWE, soil moisture, and aquifer storage).

Figure 7 also shows that the magnitude of correlations between hydrological variables and SSI-6 may vary with the analysis period, especially during exceptionally dry periods. For example, the relationships between precipitation and SSI-6 in rainfall-dominated and mixed catchments (Claro, Palos, Ñuble and Cautín) are stronger during the 1998/99 drought, with Spearman correlations near 1 in the 9-month scale, whereas the remaining periods yield correlations that do not exceed 0.7 in the same temporal scale. Considerable differences are also obtained for SWE, with high correlations (>0.7) in all basins for the 9 and 12-month temporal scales during the 1998/99 event. On the other hand, the correlations for these scales are lower over larger time windows (the whole period), whereas the correlations increase for larger scales (18 and 24 months). The selection of

the analysis period also yields evident differences in the correlation between soil moisture and aquifer storage. Indeed, higher correlations are obtained for these variables when using temporal scales shorter than 9 months, especially in Choapa and Palos, where the snowmelt contribution to runoff is substantial.

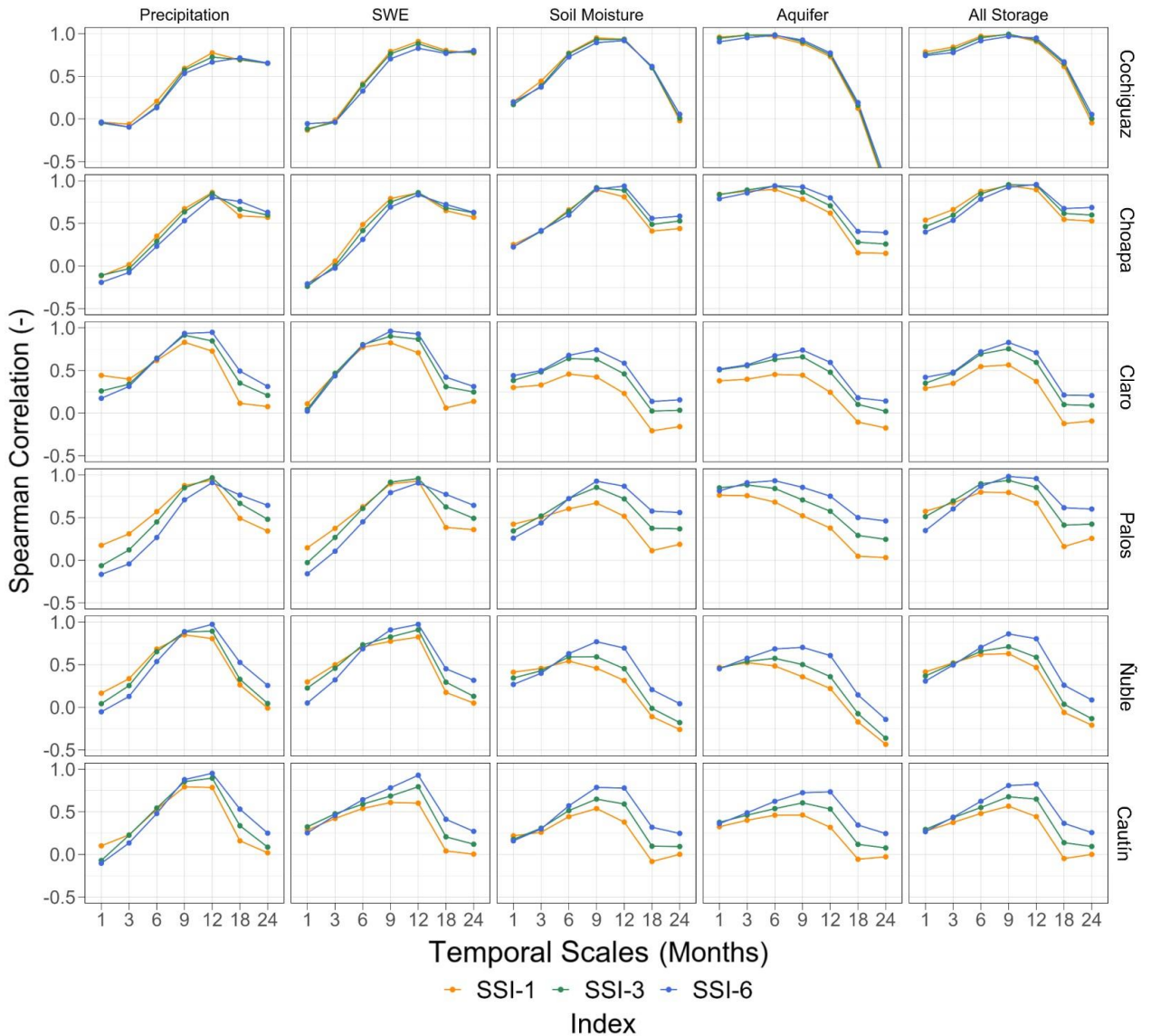


Figure 6: Spearman rank correlation coefficients between the SSI computed at different time scales (1, 3, and 6 months), and temporally aggregated/averaged hydrological variables (columns) over the period Jan/1998-Dec/2000. The results for each case study basin are displayed in different rows.

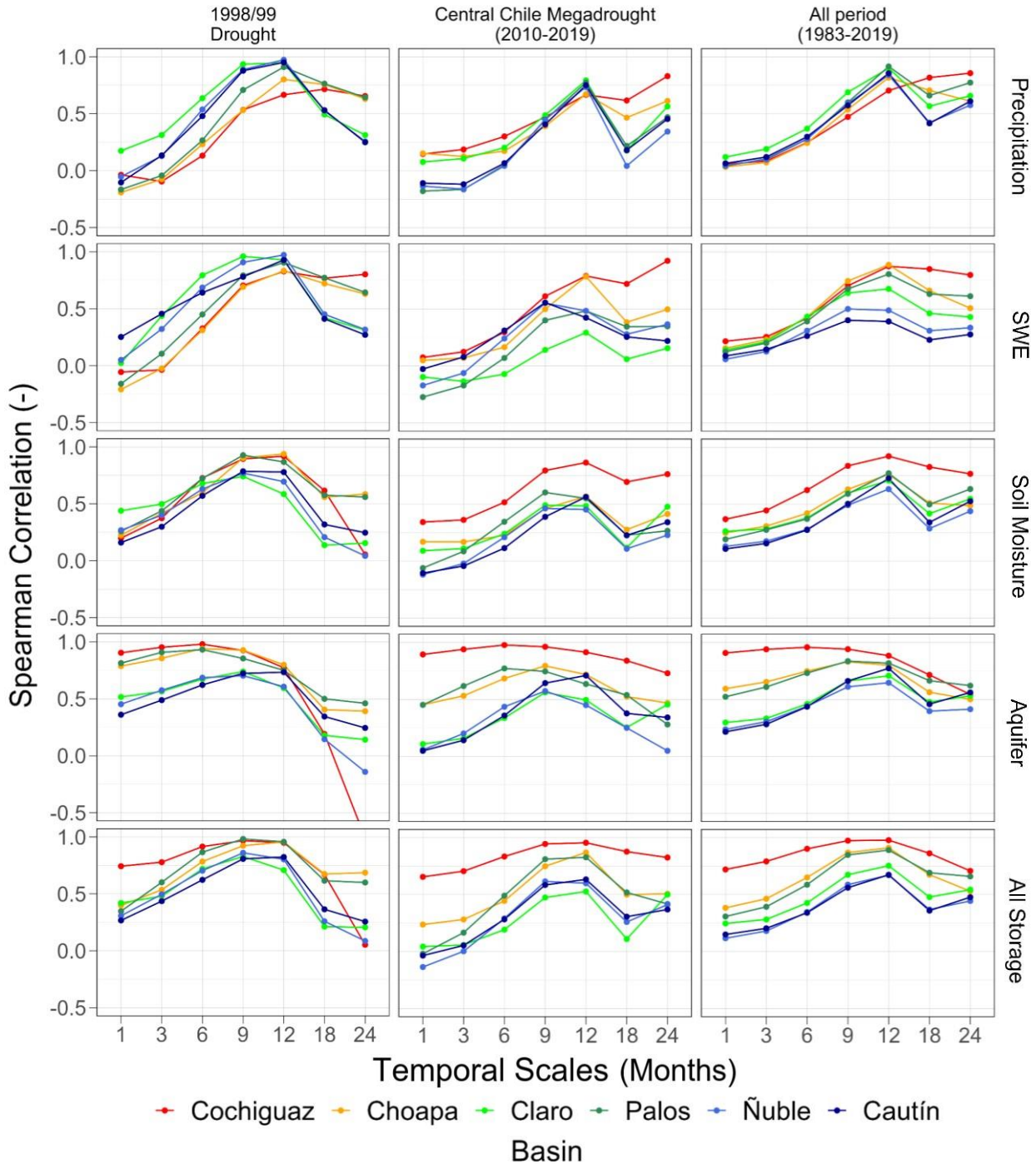


Figure 7: Spearman rank correlation coefficients between SSI-6 and temporally aggregated/averaged catchment-scale hydrological variables (rows) for three different periods: the October/1998-September/1999 drought event, (b) the central Chile megadrought (April/2010-March/2019), and (c) the entire analysis period (April/1983 - March/2020).

4.4 Effects of temporal aggregation on drought propagation

Figure 8 illustrates how the preceding correlation analysis can inform the choice of the temporal scale for the calculation of standardized indices in drought propagation studies. Specifically, Figure 8 displays time series of five standardized indices – i.e., the SPI (precipitation), SPEI (precipitation minus PET), SSMI (soil moisture), SWSI (total water storage), and the SSI –, calculated at the temporal scales at which its associated hydrologic variable maximizes its correlation compared to SSI. In particular, we display the time series for the Cautín River basin during the period April/1983-March/2020, along with the drought events recorded in 1989, 1996, 1998/99 and 2015/16. It can be noted how precipitation deficits propagate towards other catchment-scale storages, triggering soil moisture and/or hydrological droughts in some cases, which may differ in terms of duration and intensity.

To what extent can the choice of the temporal scale affect the portrayal of drought propagation across different hydrological regimes? To find answers, we examine the transition of meteorological towards soil moisture and hydrological droughts in the duration–intensity space using four different criteria, with a focus on two events – the 1998/99 and 2012–2016 droughts (a subperiod of the Chile megadrought) – that simultaneously affected the Choapa (snowmelt driven), Palos (mixed regime) and Cautín (rainfall driven) River basins (Figure 9). The same analysis was also performed for the Cochiguaz, Claro, and Ñuble River basins, which are shown in Figure S.3 of the Supplementary material. The results show that different temporal scales alter the duration and intensity, as well as the progression of such characteristics in a specific hydrological system. For example, in this study (red) we obtain that in the Palos River basin the soil column buffers the intensity of meteorological droughts, which transitions toward a shorter and more intense hydrological drought for the 1998/99 event; 1-month (purple) and 3-month (green) scales show a transition from a very intense and short meteorological drought towards a longer and smoother hydrological drought; nevertheless, the recommendation of Baez-Villanueva et al. (2023, blue) yields a decline in intensity and a slightly shorter duration from meteorological to hydrological drought. Other discrepancies in drought trajectories are obtained in all combinations of basin/event.

Note that the relative location of soil moisture drought within the trajectories can be very different depending on the temporal scale selected. An interesting example is the 2012–2016 event at the Choapa River basin, for which the four trajectories differ considerably; in particular, the temporal scales found here yield very similar durations for meteorological and hydrological droughts, and a more intense and prolonged soil moisture drought. Notably, Figure 9 also shows that our trajectories (red symbols and arrows) for the two events analyzed are similar at the Palos and Cautín River basins, suggesting a similar propagation pattern between mixed and rainfall-driven regimes. The same pattern is also obtained for the Ñuble River basin (Figure S.3 in Supplementary material).

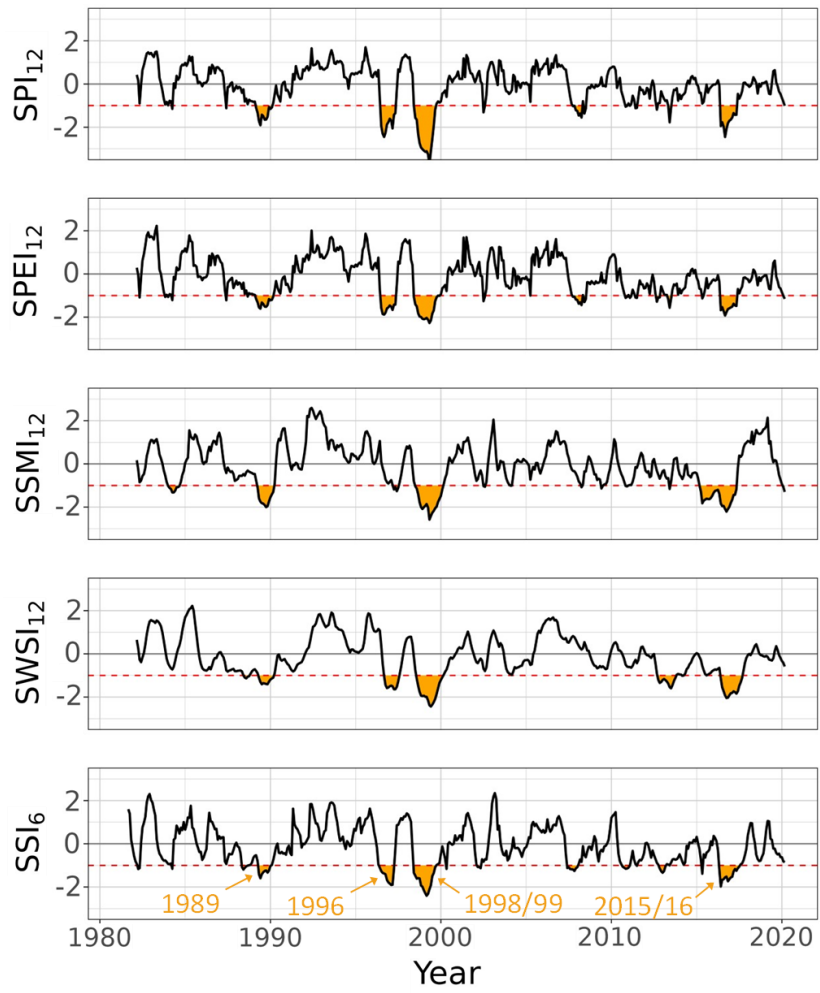


Figure 8: Monthly time series of standardized indices (period April/1983 - March/2020) at the Cautín River basin, computed with temporal scales selected from the correlation analyses conducted in this study. The yellow areas indicate the events of 1989, 1996, 1998/99 and 2015/16.

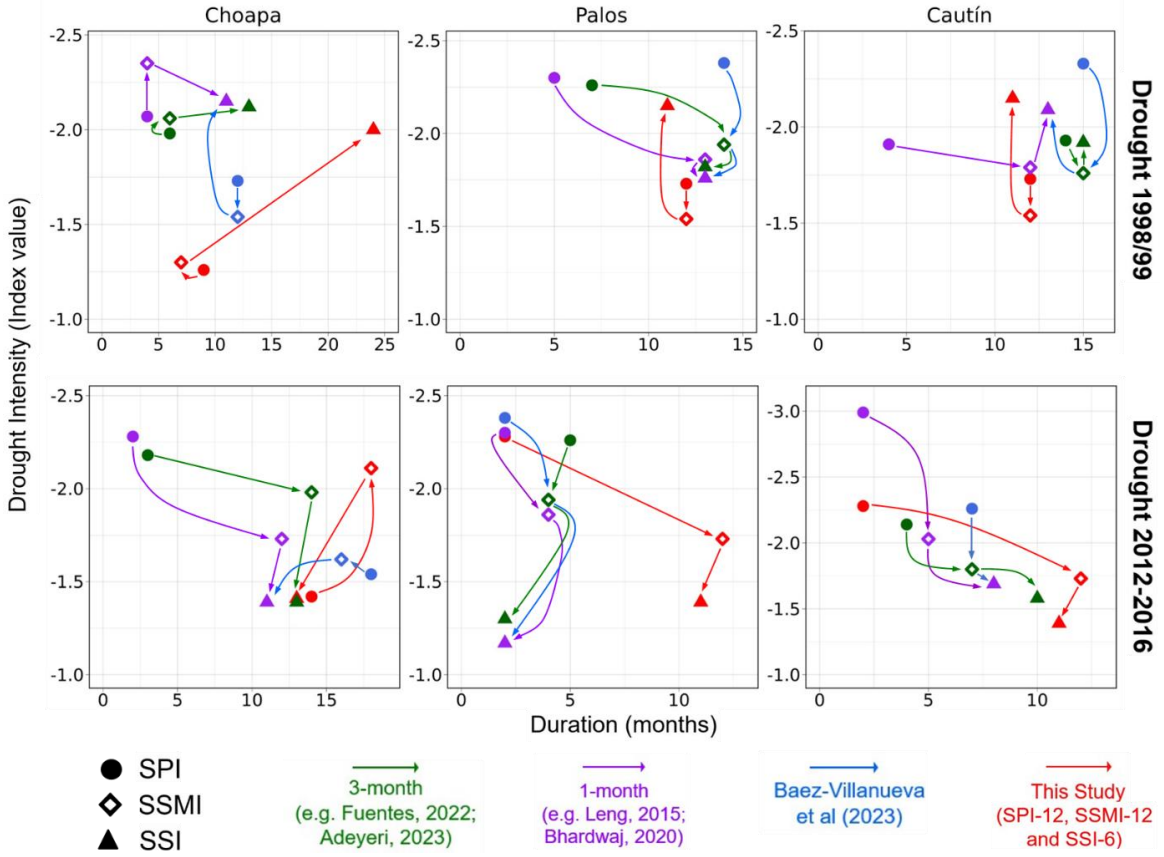


Figure 9: Propagation from meteorological (circles) to soil moisture (diamonds) and hydrological (triangles) droughts for two selected drought events (1998/99 and 2012/17, displayed in different rows) and three basins with different hydrological regimes: (a) Choapa (snowmelt-driven, left), (b) Palos (mixed regime, center) and Cautín (rainfall-driven, right). The x-axis shows the duration in months, and the y-axis displays the intensity. The colors indicate trajectories obtained with the temporal scales recommended by different studies (see text for details).

5. Discussion

5.1 Drought detection and characteristics

The results presented here reveal additional insights for hydrological drought analysis based on SSI estimates. Firstly, we show that even a 1-month scale for the SSI can distort the variability of raw monthly streamflow time series (Figure 4). Despite the results confirming well-known effects of streamflow aggregation on the frequency and duration of hydrological droughts detected with the SSI (e.g., Barker et al., 2016; Teutschbein et al., 2022), we found that such impacts are minor in slow-reacting catchments (e.g., Cochiguaz River basin, with average drought durations spanning 12.3-12.9 months), which can be explained by the buffering effect of snowpack, as well as soil moisture and aquifer storage. Conversely, the impacts of the temporal scale and duration constraints are more noticeable in basins with important rainfall contributions to runoff during winter. Note that the relatively longer average drought durations found in semi-arid, snowmelt-driven catchments (which also hold the largest baseflow contributions) align well with previous

studies linking drought duration with catchment storage properties (A. F. Van Loon & Laaha, 2015; Barker et al., 2016).

5.2 Drivers of the SSI across hydrological regimes

In rainfall-driven basins, we found a strong connection between the SSI-6 and precipitation (i.e., a strong link between hydrological and meteorological drought), whereas storages – especially soil moisture and aquifer – become more important in basins with increased aridity, in agreement with previous studies (e.g., Haslinger et al., 2014; Barker et al., 2016). Our results also show that dependencies between correlations and hydroclimatic regimes may change during the analysis period (Figure 7), highlighting the uniqueness of each drought event.

We show that aggregating streamflow into seasonal periods (i.e., 3 and 6 months) for SSI calculations does not necessarily attenuate potential relationships with other water cycle variables (see snowmelt-driven basins in Figure 4). Even more, shifting from SSI-1 to SSI-3 and SSI-6 enhances the explanatory power of soil moisture and aquifer storage for nearly all temporal scales in mixed and rainfall-driven regime basins, which means that the SSI reflects – in addition to long-lasting streamflow anomalies (Seibert et al., 2017; Deutschbein et al., 2022) – the delayed signal in such storages reaching the catchment outlet. These results suggest that the temporal scale used for the SSI should be selected based on the specific purposes and the hydroclimatic regime if the aim is to enhance the interpretability of physical mechanisms.

Although previous studies have shown that meteorological droughts may propagate differently depending on hydroclimatic characteristics and system properties (e.g., Van Loon et al., 2014; Van Loon & Laaha, 2015; Barker et al., 2016; Apurv et al., 2017), we show that such portrayal may be very sensitive – for a given combination of event and catchment – to the subjective choice of the temporal scale used to compute standardized indices (Figure 9). Moreover, given a well-defined criterion to compute standardized indices (in this study: SPI-12, SSMI-12, and SSI-6), the trajectories of the same drought event may differ considerably among catchments. Likewise, propagation trajectories can differ substantially among drought events within a particular catchment. This is shown in Figure S.4 of the Supplementary material. Overall, this work suggests that any results derived from standardized indices should be interpreted cautiously.

5.3 Limitations and future work

A key aspect of our methodology is the identification of controls (and associated temporal scales) driving fluctuations in the SSI through variables simulated with a calibrated, state-of-the-art process-based hydrological model. This approach departs from previous efforts searching for statistical relationships with standardized indices such as the SPI (e.g., Barker et al., 2016; Huang et al., 2017; Wu et al., 2022), the SPEI (e.g., Peña-Gallardo et al., 2019; Wang et al., 2020; Bevacqua et al., 2021), or other indices and state variables derived from reanalysis datasets that do not necessarily correspond to observed streamflow anomalies (e.g., Hoffmann et al., 2020). However, we did not consider in-situ or remotely-sensed observations of SWE, soil moisture, and aquifer storage in the calibration process, relying on the capability of the SUMMA model to replicate streamflow signatures.

Future work could expand the analyses presented in this study by exploring tradeoffs between the temporal scales used to compute the SSI and the choice of statistical distributions (e.g., Svensson et al., 2017; Teutschbein et al., 2022) or threshold selection approach (e.g., Wanders et al., 2015; Odongo et al., 2023). Finally, although our results align well with previous studies connecting drought characteristics with climate and catchment descriptors, a larger number of basins would enable more robust conclusions for mountainous basins.

6. Conclusions

The standardized streamflow index (SSI) has been widely used for hydrological drought monitoring, forecasting, and propagation analyses. Nevertheless, there is limited understanding of the effects that the subjective choice of temporal scales may exert on the characterization of these events and, more importantly, on which hydrological variables the SSI fluctuations are predominantly related. In this study, we intend to fill these gaps by applying the SUMMA model, coupled with the mizuRoute routing model, in six hydroclimatically different basins located on the western slopes of the extratropical Andes. We also illustrate how sensitive the portrayal of drought propagation is to the temporal scales used to compute popular standardized indices such as the SPI and the SSMI. Our main findings are as follows:

1. The temporal scale used to compute the SSI and the minimum duration to define hydrological drought occurrence can largely affect the events estimated duration and frequency, especially in rainfall-driven catchments.
2. The strength of the relationship between the SSI and hydrological variables is less affected by the choice of temporal scales of the SSI in snow-driven regimes compared to mixed and rainfall-dominated basins, where the dispersion of correlations progressive increases when evaluating the indices on scales larger than nine months.
3. Higher correlations are achieved when SSI-6 is contrasted against hydrological variables temporally aggregated at 9 and 12 months – except for aquifer storage at the Cochiguaz basin (snow-driven) –, and decrease for temporal scales larger than 12 months. When the SSI-1 and SSI-3 are used, the correlations are maximized at shorter temporal scales (compared to the SSI-6) for some combinations of hydrological variables and basins (e.g., aquifer storage at Palos and Ñuble).
4. When analyzing the entire period, higher correlations between the SSI-6 and hydrological variables are achieved for snowmelt-driven basins, and these progressively decrease towards rainfall-driven regimes. This pattern becomes stronger when the total amount of storage within a basin is considered. Nevertheless, such a pattern becomes less clear and dependent on the temporal aggregation of explanatory variables during drought periods.
5. The portrayal of drought propagation may change drastically depending on the subjective choice of the temporal aggregation used to compute standardized indices, even if the same dataset. In this regard, different criteria may reveal opposite trajectories of drought propagation for the same event in a basin.

Acknowledgments

Fabián Lema, Pablo A. Mendoza, and Nicolás Vásquez were supported by Fondecyt Project 11200142. P. A. Mendoza also received financial support from CONICYT/PIA Project AFB180004. Nicolás Vásquez also received support from the Emerging Leaders in the Americas Program (ELAP) scholarship (Canada) and the ANID Doctorado Nacional scholarship No. 21230289 (Chile).

Powered@NLHPC: This research was partially supported by the supercomputing infrastructure of the NLHPC (ECM-02).

List of figures

Figure 1: Location and seasonal variability of precipitation (P), runoff (Q) and temperature for the six case study basins: (a) Cochiguaz River at El Peñón, (b) Choapa River at Cuncumén, (c) Claro River at El Valle, (d) Palos River at Colorado, (e) Ñuble River at La Punilla, and (f) Cautín River at Rari-Ruca.....	8
Figure 2: Flowchart describing the approach used in this study.	10
Figure 3: Comparison between simulated and observed streamflow for all basins in terms of (a) daily time series (April/2014 to March/2020), (b) daily flow duration curves (vertical logarithmic scale), and (c) mean monthly runoff.	14
Figure 4: Monthly time series of (a) precipitation, (b) SPI, (c) SWE, (d) total soil moisture, (e) aquifer storage, (f) streamflow, and (g) SSI for the Choapa (snowmelt-driven, left) and Cautín (rainfall-driven, right) River basins.	15
Figure 5: Effects of the choice of temporal scale (1, 3, and 6 months) in SSI calculations and duration restrictions on (a) the frequency and (b,c) duration of hydrological droughts detected between the water years 1983/84-2019/20.	17
Figure 6: Spearman rank correlation coefficients between the SSI computed at different time scales (1, 3, and 6 months), and temporally aggregated/averaged hydrological variables (columns) over the period Jan/1998-Dec/2000.....	19
Figure 7: Spearman rank correlation of coefficients between SSI-6 and temporally aggregated/averaged catchment-scale hydrological variables (rows) for three different periods: the October/1998-September/1999 drought event, (b) the central Chile megadrought (April/2010-March/2019), and (c) the entire analysis period (April/1983 - March/2020).	20
Figure 8: Monthly time series of standardized indices (period April/1983 - March/2020) at the Cautín River basin, computed with temporal scales selected from the correlation analyses conducted in this study.....	22
Figure 9: Propagation from meteorological (circles) to soil moisture (diamonds) and hydrological (triangles) droughts for two selected drought events (1998/99 and 2016/17, displayed in different rows) and three basins with different hydrological regimes: (a) Choapa (snowmelt-driven, left), (b) Palos (mixed regime, center) and Cautín (rainfall-driven, right).	23

List of tables

Table 1: Physiographic and climate attributes of the six basins considered in this study. All data came from CAMELS-CL database, except for the baseflow index, which was estimated from hydrological simulations in SUMMA model.....	8
Table 2: Mean duration of drought events for each case and temporal aggregation of SSI.....	17

Capítulo 3: Conclusiones

En este trabajo, se presenta un análisis crítico del Índice Estandarizado de Caudal (SSI por sus siglas en inglés), describiéndose las implicancias de la elección de la escala temporal en la detección y caracterización de eventos de sequía. El SSI ha sido ampliamente utilizado en estudios hidrológicos, abarcando temáticas como el monitoreo, predicción y análisis de propagación de sequías. Sin embargo, existe un conocimiento limitado sobre cuáles son las variables hidrológicas con las que este índice se correlaciona y la influencia que generan factores como el régimen hidrológico de las cuencas.

Para contribuir a un mayor entendimiento de este índice, se implementó el modelo hidrológico SUMMA, acoplado al modelo de rastreo de caudales mizuRoute, en seis cuencas con diferente régimen hidrológico en Chile Central, estimando y evaluando la relación existente entre distintas variables hidrológicas, el SSI y otros índices estandarizados. También se analizó el efecto causado por el cálculo de índices – estimados en diferentes escalas temporales – sobre la duración y frecuencia de los eventos de sequía detectados en cada caso. Finalmente, se comparó la trayectoria de propagación de sequías obtenida en este estudio – a partir de los índices mutuamente correlacionados – con otras estimadas mediante el uso de criterios comúnmente usados en la literatura, basadas en el uso de distintas agregaciones temporales de índices estandarizados

Los principales hallazgos que se obtuvieron en este trabajo son:

1. Existen al menos dos aspectos claves que influyen considerablemente en la detección de eventos de sequías por medio del SSI. Por un lado, resulta relevante la escala temporal escogida para su cálculo, mientras que también impacta la decisión de escoger algún tipo de restricción asociada a una duración mínima del evento. Ambos factores afectan la frecuencia y duración promedio de los eventos, en especial sobre cuencas de régimen pluvial.
2. En las cuencas que presentan una importante componente nival, se encontraron pocas variaciones en las correlaciones obtenidas con el índice SSI agregado a 1, 3 y 6 meses. Lo anterior contrasta drásticamente con los resultados obtenidos en cuencas de régimen pluvio-nival y pluvial, donde se evidencia un progresivo incremento en la dispersión de correlaciones al analizar escalas temporales mayores a 9 meses.
3. En general, las mayores correlaciones se obtuvieron cuando el índice SSI-6 se contrastó con variables hidrológicas agregadas a una escala entre 9 y 12 meses, disminuyendo al evaluar en escalas temporales mayores y existiendo algunas excepciones, como el almacenamiento del acuífero en la cuenca del río Cochiguaz (nival). Asimismo, este mismo almacenamiento, obtenido con escalas menores a 9 meses, se correlaciona mejor con los índices SSI-1 y SSI-3 en comparación al SSI-6.
4. Entre las cuencas analizadas, aquellas de régimen nival son las que entregaron las mayores correlaciones entre los almacenamientos y el SSI, relación que va disminuyendo de forma progresiva en cuencas en que la componente pluvial se vuelve más relevante para la generación de escorrentía. Este patrón, que sigue un gradiente hidroclimático, es particularmente notorio

al analizar el almacenamiento total y se hace más débil al evaluar períodos de sequía específicos.

5. El uso de distintos criterios en el cálculo de índices estandarizados puede generar resultados drásticamente diferentes sobre el análisis de propagación de sequías – desde una meteorológica hacia sequías de humedad del suelo e hidrológica –, indicando en algunos casos direcciones opuestas – intensificación o amortiguación del evento de sequía – para un mismo evento y una misma cuenca. Estas discrepancias ocurren incluso si se utiliza el mismo set de datos.

Bibliografía

- Adeyeri, O. E., Zhou, W., Laux, P., Ndehedehe, C. E., Wang, X., Usman, M., & Akinsanola, A. A. (2023). Multivariate Drought Monitoring, Propagation, and Projection Using Bias-Corrected General Circulation Models. *Earth's Future*, 11(4), 1–16. <https://doi.org/10.1029/2022EF003303>
- Alvarez-Garreton, C., Mendoza, P. A., Boisier, J. P., Addor, N., Galleguillos, M., Zambrano-Bigiarini, M., et al. (2018). The CAMELS-CL dataset: catchment attributes and meteorology for large sample studies – Chile dataset. *Hydrology and Earth System Sciences*, 22(11), 5817–5846. <https://doi.org/10.5194/hess-22-5817-2018>
- Andreadis, K. M., Clark, E. A., Wood, A. W., Hamlet, A. F., & Lettenmaier, D. P. (2005). Twentieth-century drought in the conterminous United States. *Journal of Hydrometeorology*, 6(6), 985–1001. <https://doi.org/10.1175/JHM450.1>
- Apurv, T., Sivapalan, M., & Cai, X. (2017). Understanding the Role of Climate Characteristics in Drought Propagation. *Water Resources Research*, 53(11), 9304–9329. <https://doi.org/10.1002/2017WR021445>
- Bachmair, S., Kohn, I., & Stahl, K. (2015). Exploring the link between drought indicators and impacts. *Natural Hazards and Earth System Sciences*, 15(6), 1381–1397. <https://doi.org/10.5194/nhess-15-1381-2015>
- Baez-Villanueva, O. M., Zambrano-bigiarini, M., Miralles, D. G., Beck, H. E., Siegmund, J. F., Alvarez-garreton, C., et al. (2023). On the time scale of meteorological, soil moisture, and snow drought indices to assess streamflow drought over catchments with different hydrological regime: a case study using a hundred Chilean catchments, (August), 1–34.
- Barker, L. J., Hannaford, J., Chiverton, A., & Svensson, C. (2016). From meteorological to hydrological drought using standardised indicators. *Hydrology and Earth System Sciences*, 20(6), 2483–2505. <https://doi.org/10.5194/hess-20-2483-2016>
- Beguería, S., Vicente-Serrano, S. M., Reig, F., & Latorre, B. (2014). Standardized precipitation evapotranspiration index (SPEI) revisited: parameter fitting, evapotranspiration models, tools, datasets and drought monitoring. *International journal of climatology*, 34(10), 3001-3023
- Bevacqua, A. G., Chaffe, P. L. B., Chagas, V. B. P., & AghaKouchak, A. (2021). Spatial and temporal patterns of propagation from meteorological to hydrological droughts in Brazil. *Journal of Hydrology*, 603(PA), 126902. <https://doi.org/10.1016/j.jhydrol.2021.126902>
- Bhardwaj, K., Shah, D., Aadhar, S., & Mishra, V. (2020). Propagation of Meteorological to Hydrological Droughts in India. *Journal of Geophysical Research: Atmospheres*, 125(22). <https://doi.org/10.1029/2020JD033455>
- Boisier, J. P., R. Rondanelli, R. D. Garreaud, and F. Muñoz (2016), Anthropogenic and natural contributions to the Southeast Pacific precipitation decline and recent megadrought in central Chile, *Geophys. Res. Lett.*, 43, 413–421, doi:10.1002/2015GL067265

- Brunner, L., Pendergrass, A. G., Lehner, F., Merrifield, A. L., Lorenz, R., & Knutti, R. (2020). Reduced global warming from CMIP6 projections when weighting models by performance and independence. *Earth System Dynamics*, 11(4), 995–1012. <https://doi.org/10.5194/esd-11-995-2020>
- Brunner, M. I., & Tallaksen, L. M. (2019). Proneness of European Catchments to Multiyear Streamflow Droughts. *Water Resources Research*, 55(11), 8881–8894. <https://doi.org/10.1029/2019WR025903>
- Buitink, J., van Hateren, T. C., & Teuling, A. J. (2021). Hydrological System Complexity Induces a Drought Frequency Paradox. *Frontiers in Water*, 3(May), 1–12. <https://doi.org/10.3389/frwa.2021.640976>
- Carrao, H., Russo, S., Sepulcre, G., & Barbosa, P. (2013, December). Agricultural Drought Assessment In Latin America Based On A Standardized Soil Moisture Index. In ESA Living Planet Symposium (Vol. 722, p. 127).
- Celia, M. A., E. T. Bouloutas, and R. L. Zarba (1990), A general mass-conservative numerical solution for the unsaturated flow equation, *Water Resources Research*, 26 (7), 1483-1496, doi: 10.1029/90wr00196
- Clark, M. P., Nijssen, B., Lundquist, J. D., Kavetski, D., Rupp, D. E., Woods, R. A., Freer, J. E., Gutmann, E. D., Wood, A. W., Brekke, L. D., et al. (2015a). A unified approach for process-based hydrologic modeling: 1. Modeling concept. *Water Resources Research*. <https://doi.org/10.1002/2015WR017198>
- Clark, M. P., Nijssen, B., Lundquist, J. D., Kavetski, D., Rupp, D. E., Woods, R. A., Freer, J. E., Gutmann, E. D., Wood, A. W., Gochis, D. J., et al. (2015b). A unified approach for process-based hydrologic modeling: 2. Model implementation and case studies. *Water Resources Research*. <https://doi.org/10.1002/2015WR017200>
- Clark, M. P., Zolfaghari, R., Green, K. R., Trim, S., Knoben, W. J. M., Bennett, A., et al. The numerical implementation of land models: Problem formulation and laugh tests, 22 *Journal of Hydrometeorology* § (2021). <https://doi.org/10.1175/JHM-D-20-0175.1>
- Cook, B. I., Smerdon, J. E., Seager, R., & Coats, S. (2014). Global warming and 21st century drying. *Climate Dynamics*, 43(9–10), 2607–2627. <https://doi.org/10.1007/s00382-014-2075-y>
- DGA. (2017). Actualización del balance hídrico nacional, SIT N°417. Ministerio de Obras Públicas, Dirección General de Aguas, División de Estudios y Planificación.
- Fowé, T., Yonaba, R., Mounirou, L. A., Ouédraogo, E., Ibrahim, B., Niang, D., et al. (2023). From meteorological to hydrological drought: a case study using standardized indices in the Nakanbe River Basin, Burkina Faso. *Natural Hazards*, (0123456789). <https://doi.org/10.1007/s11069-023-06194-5>
- Garcia, F., Folton, N., & Oudin, L. (2017). Which objective function to calibrate rainfall-runoff models for low-flow index simulations? *Hydrological Sciences Journal*, 62(7), 1149–1166.

<https://doi.org/10.1080/02626667.2017.1308511>

- Garreaud, R., Alvarez-Garreton, C., Barichivich, J., Pablo Boisier, J., Christie, D., Galleguillos, M., et al. (2017). The 2010–2015 megadrought in central Chile: Impacts on regional hydroclimate and vegetation. *Hydrology and Earth System Sciences*, 21(12), 6307–6327. <https://doi.org/10.5194/hess-21-6307-2017>
- Garreaud, R. D., Boisier, J. P. P., Rondanelli, R., Montecinos, A., Sepúlveda, H. H. H., & Veloso-Aguila, D. (2019). The Central Chile Mega Drought (2010–2018): A climate dynamics perspective. *International Journal of Climatology*, 40(June), 1–19. <https://doi.org/10.1002/joc.6219>
- Gupta, H. V., Kling, H., Yilmaz, K. K., & Martinez, G. F. (2009). Decomposition of the mean squared error and NSE performance criteria: Implications for improving hydrological modelling. *Journal of Hydrology*, 377(1–2), 80–91. <https://doi.org/10.1016/j.jhydrol.2009.08.003>
- Hansen, G., & Stone, D. (2016). Assessing the observed impact of anthropogenic climate change. *Nature Climate Change*, 6(5), 532–537
- Hameed, M. M., Mohd Razali, S. F., Wan Mohtar, W. H. M., & Yaseen, Z. M. (2023). Improving multi-month hydrological drought forecasting in a tropical region using hybridized extreme learning machine model with Beluga Whale Optimization algorithm. *Stochastic Environmental Research and Risk Assessment*, 37(12), 4963–4989. <https://doi.org/10.1007/s00477-023-02548-4>
- Haslinger, K., Koffler, D., Schöner, W., & Laaha, G. (2014). Exploring the link between meteorological drought and streamflow: Effects of climate–catchment interaction. *Water Resources Research*, 50(3), 2468–2487. <https://doi.org/10.1002/2013WR015051>
- Hoffmann, D., Gallant, A. J. E., & Arblaster, J. M. (2020). Uncertainties in Drought From Index and Data Selection. *Journal of Geophysical Research: Atmospheres*, 125(18), 1–21. <https://doi.org/10.1029/2019JD031946>
- Huang, S., Li, P., Huang, Q., Leng, G., Hou, B., & Ma, L. (2017). The propagation from meteorological to hydrological drought and its potential influence factors. *Journal of Hydrology*, 547, 184–195. <https://doi.org/10.1016/j.jhydrol.2017.01.041>
- Jarvis, P. (1976), The interpretation of the variations in leaf water potential and stomatal conductance found in canopies in the field, Philosophical Transactions of the Royal Society of London. B, Biological Sciences, 273 (927), 593–610, doi: 10.1098/rstb.1976.0035
- Jordan, R. (1991), A one-dimensional temperature model for a snow cover. Technical documentation for SNTERM.89, 49 pp, U.S. Army Corps of Engineers Cold Regions Research and Engineering Laboratory.
- Laimighofer, J., & Laaha, G. (2022). How standard are standardized drought indices? Uncertainty components for the SPI & SPEI case. *Journal of Hydrology*, 613, 128385

- Lee, J., Kim, Y., & Wang, D. (2022). Assessing the characteristics of recent drought events in South Korea using WRF-Hydro. *Journal of Hydrology*, 607(December 2021), 127459. <https://doi.org/10.1016/j.jhydrol.2022.127459>
- Liang, X., Wood, E. F., & Lettenmaier, D. P. (1996). Surface soil moisture parameterization of the VIC-2L model: Evaluation and modification. *Global and Planetary Change*, 13(1-4), 195-206
- Mahat, V., and D. G. Tarboton (2012), Canopy radiation transmission for an energy balance snowmelt model, *Water Resources Research*, 48, doi: W01534, 10.1029/2011wr010438
- Mahat, V., D. G. Tarboton, and N. P. Molotch (2013), Testing above- and below-canopy representations of turbulent fluxes in an energy balance snowmelt model, *Water Resources Research*, 49 (2), 1107-1122, doi:10.1002/wrcr.20073
- Matott, L. (2017). OSTRICH: an Optimization Software Tool, Documentation and User's Guide, Version 17.12.19
- McKee, T. B., Doesken, N. J., & John, K. (1993). The relationship of drought frequency and duration to time scales. In *Eighth Conference on Applied Climatology*. Anaheim, California.
- Mizukami, N., Clark, M. P., Sampson, K., Nijssen, B., Mao, Y., McMillan, H., et al. (2016). mizuRoute version 1: a river network routing tool for a continental domain water resources applications. *Geoscientific Model Development*, 9(6), 2223–2238. <https://doi.org/10.5194/gmd-9-2223-2016>
- Mizukami, N., Clark, M. P., Gharari, S., Kluzek, E., Pan, M., Lin, P., et al. (2021). A Vector-Based River Routing Model for Earth System Models: Parallelization and Global Applications. *Journal of Advances in Modeling Earth Systems*, 13(6), 1–20. <https://doi.org/10.1029/2020MS002434>
- Modarres, R. (2007). Streamflow drought time series forecasting. *Stochastic Environmental Research and Risk Assessment*, 21(3), 223–233. <https://doi.org/10.1007/s00477-006-0058-1>
- Nash, J., & Sutcliffe, J. (1970). River flow forecasting through conceptual models part I - A discussion of principles. *Journal of Hydrology*, 10(3), 282–290. [https://doi.org/10.1016/0022-1694\(70\)90255-6](https://doi.org/10.1016/0022-1694(70)90255-6)
- Niu, G. Y., Z. L. Yang, K. E. Mitchell, F. Chen, M. B. Ek, M. Barlage, A. Kumar, K. Manning, D. Niyogi, E. Rosero, M. Tewari, and Y. L. Xia (2011), The community Noah land surface model with multiparameterization options (Noah-MP): 1. Model description and evaluation with local-scale measurements, *Journal of Geophysical Research-Atmospheres*, 116, doi: D12109, 10.1029/2010jd015139
- Nkiaka, E., Nawaz, N. R., & Lovett, J. C. (2017). Using standardized indicators to analyse dry/wet conditions and their application for monitoring drought/floods: a study in the Logone catchment, Lake Chad basin. *Hydrological Sciences Journal*, 62(16), 2720–2736. <https://doi.org/10.1080/02626667.2017.1409427>
- Núñez, J., Rivera, D., Oyarzún, R., & Arumí, J. L. (2014). On the use of Standardized Drought

Indices under decadal climate variability: Critical assessment and drought policy implications. *Journal of Hydrology*, 517, 458–470. <https://doi.org/10.1016/j.jhydrol.2014.05.038>

- Odongo, R. A., De Moel, H., & Van Loon, A. F. (2023). Propagation from meteorological to hydrological drought in the Horn of Africa using both standardized and threshold-based indices. *Natural Hazards and Earth System Sciences*, 23(6), 2365–2386. <https://doi.org/10.5194/nhess-23-2365-2023>
- Oertel, M., Meza, F. J., & Gironás, J. (2020). Observed trends and relationships between ENSO and standardized hydrometeorological drought indices in central Chile. *Hydrological Processes*, 34(2), 159–174. <https://doi.org/10.1002/hyp.13596>
- Okumura, Y. M., DiNezio, P., & Deser, C. (2017). Evolving Impacts of Multiyear La Niña Events on Atmospheric Circulation and U.S. Drought. *Geophysical Research Letters*, 44(22), 11,614–11,623. <https://doi.org/10.1002/2017GL075034>
- Peña-Gallardo, M., Vicente-Serrano, S. M., Hannaford, J., Lorenzo-Lacruz, J., Svoboda, M., Domínguez-Castro, F., et al. (2019). Complex influences of meteorological drought time-scales on hydrological droughts in natural basins of the contiguous United States. *Journal of Hydrology*, 568(November 2018), 611–625. <https://doi.org/10.1016/j.jhydrol.2018.11.026>
- Peters-Lidard, C. D., Mocko, D. M., Su, L., Lettenmaier, D. P., Gentine, P., & Barlage, M. (2021). Advances in land surface models and indicators for drought monitoring and prediction. *Bulletin of the American Meteorological Society*, 102(5), E1099–E1122. <https://doi.org/10.1175/BAMS-D-20-0087.1>
- Pokhrel, Y., Felfelani, F., Satoh, Y., Boulange, J., Burek, P., Gädeke, A., et al. (2021). Global terrestrial water storage and drought severity under climate change. *Nature Climate Change*, 11(3), 226–233. <https://doi.org/10.1038/s41558-020-00972-w>
- Rakovec, O., Samaniego, L., Hari, V., Markonis, Y., Moravec, V., Thober, S., et al. (2022). The 2018–2020 Multi-Year Drought Sets a New Benchmark in Europe. *Earth's Future*, 10(3), 1–11. <https://doi.org/10.1029/2021EF002394>
- Raupach, M. (1994). Simplified expressions for vegetation roughness length and zero-plane displacement as functions of canopy height and area index, *Boundary-Layer Meteorology*, 71 (1-2), 211-216, doi:10.1007/bf00709229
- Rivera, J. A., Otta, S., Lauro, C., & Zazulie, N. (2021). A Decade of Hydrological Drought in Central-Western Argentina. *Frontiers in Water*, 3(April), 1–20. <https://doi.org/10.3389/frwa.2021.640544>
- Rosenzweig, C., & Neofotis, P. (2013). Detection and attribution of anthropogenic climate change impacts. *Wiley Interdisciplinary Reviews: Climate Change*, 4(2), 121–150.
- Samaniego, L., Kumar, R., & Zink, M. (2013). Implications of parameter uncertainty on soil moisture drought analysis in Germany. *Journal of Hydrometeorology*, 14(1), 47–68. <https://doi.org/10.1175/JHM-D-12-075.1>

- Schumacher, D. L., Keune, J., Dirmeyer, P., & Miralles, D. G. (2022). Drought self-propagation in drylands due to land–atmosphere feedbacks. *Nature Geoscience*, 15(4), 262–268. <https://doi.org/10.1038/s41561-022-00912-7>
- Seibert, M., Merz, B., & Apel, H. (2017). Seasonal forecasting of hydrological drought in the Limpopo Basin: a comparison of statistical methods. *Hydrology and Earth System Sciences*, 21(3), 1611–1629. <https://doi.org/10.5194/hess-21-1611-2017>
- Sheffield, J., & Wood, E. F. (2007). Characteristics of global and regional drought, 1950–2000: Analysis of soil moisture data from off-line simulation of the terrestrial hydrologic cycle. *Journal of Geophysical Research Atmospheres*, 112(17). <https://doi.org/10.1029/2006JD008288>
- Shukla, S., & Wood, A. W. (2008). Use of a standardized runoff index for characterizing hydrologic drought. *Geophysical Research Letters*, 35(2), 1–7. <https://doi.org/10.1029/2007GL032487>
- Stahl, K., Vidal, J. P., Hannaford, J., Tijdeman, E., Laaha, G., Gauster, T., & Tallaksen, L. M. (2020). The challenges of hydrological drought definition, quantification and communication: An interdisciplinary perspective. *Proceedings of the International Association of Hydrological Sciences*, 383, 291–295. <https://doi.org/10.5194/piahs-383-291-2020>
- Steiger, N. J., Smerdon, J. E., Seager, R., Williams, A. P., & Varuolo-Clarke, A. M. (2021). ENSO-driven coupled megadroughts in North and South America over the last millennium. *Nature Geoscience*, 14(10), 739–744. <https://doi.org/10.1038/s41561-021-00819-9>
- Sutanto, Samuel J., & Van Lanen, H. A. J. (2021). Streamflow drought: Implication of drought definitions and its application for drought forecasting. *Hydrology and Earth System Sciences*, 25(7), 3991–4023. <https://doi.org/10.5194/hess-25-3991-2021>
- Sutanto, Samuel Jonson, & Van Lanen, H. A. J. (2022). Catchment memory explains hydrological drought forecast performance. *Scientific Reports*, 12(1), 1–11. <https://doi.org/10.1038/s41598-022-06553-5>
- Svensson, C., Hannaford, J., & Prosdocimi, I. (2017). Statistical distributions for monthly aggregations of precipitation and streamflow in drought indicator applications. *Water Resources Research*, 53(2), 999–1018. <https://doi.org/10.1002/2016WR019276>
- Tallaksen, L. M., & Van Lanen, H. A. J. (2004). *Hydrological Drought: Processes and Estimation Methods for Streamflow and Groundwater*.
- Teutschbein, C., Quesada Montano, B., Todorović, A., & Grabs, T. (2022). Streamflow droughts in Sweden: Spatiotemporal patterns emerging from six decades of observations. *Journal of Hydrology: Regional Studies*, 42(June). <https://doi.org/10.1016/j.ejrh.2022.101171>
- Thorntwaite, C. W. (1948). An approach toward a rational classification of climate. *Geographical review*, 38(1), 55–94.
- Tijdeman, E., Stahl, K., & Tallaksen, L. M. (2020). Drought Characteristics Derived Based on the

Standardized Streamflow Index: A Large Sample Comparison for Parametric and Nonparametric Methods. *Water Resources Research*, 56(10).
<https://doi.org/10.1029/2019WR026315>

Tokarska, K. B., Stolpe, M. B., Sippel, S., Fischer, E. M., Smith, C. J., Lehner, F., & Knutti, R. (2020). Past warming trend constrains future warming in CMIP6 models. *Science Advances*, 6(12), 1–14. <https://doi.org/10.1126/sciadv.aaz9549>

Tolson, B. A., & Shoemaker, C. A. (2007). Dynamically dimensioned search algorithm for computationally efficient watershed model calibration. *Water Resources Research*, 43(1), 1–16. <https://doi.org/10.1029/2005WR004723>

Trenberth, K. E., Dai, A., Van Der Schrier, G., Jones, P. D., Barichivich, J., Briffa, K. R., & Sheffield, J. (2014). Global warming and changes in drought. *Nature Climate Change*, 4(1), 17–22. <https://doi.org/10.1038/nclimate2067>

Van Loon, A. F., & Laaha, G. (2015). Hydrological drought severity explained by climate and catchment characteristics. *Journal of Hydrology*, 526, 3–14. <https://doi.org/10.1016/j.jhydrol.2014.10.059>

Van Loon, A. F., & Van Lanen, H. A. J. (2012). A process-based typology of hydrological drought. *Hydrology and Earth System Sciences*, 16(7), 1915–1946. <https://doi.org/10.5194/hess-16-1915-2012>

Van Loon, A. F., Tijdeman, E., Wanders, N., Van Lanen, H. A. J., Teuling, A. J., & Uijlenhoet, R. (2014). How climate seasonality modifies drought duration and deficit. *Journal of Geophysical Research*, 119(8), 4640–4656. <https://doi.org/10.1002/2013JD020383>

Van Loon, Anne F. (2015). Hydrological drought explained. *Wiley Interdisciplinary Reviews: Water*, 2(4), 359–392. <https://doi.org/10.1002/WAT2.1085>

Vicente-Serrano, S. M., Beguería, S., & López-Moreno, J. I. (2010). A multiscalar drought index sensitive to global warming: The standardized precipitation evapotranspiration index. *Journal of Climate*, 23(7), 1696–1718. <https://doi.org/10.1175/2009JCLI2909.1>

Vicente-Serrano, S. M., López-Moreno, J. I., Beguería, S., Lorenzo-Lacruz, J., Azorin-Molina, C., & Morán-Tejeda, E. (2012). Accurate Computation of a Streamflow Drought Index. *Journal of Hydrologic Engineering*, 17(2), 318–332. [https://doi.org/10.1061/\(asce\)he.1943-5584.0000433](https://doi.org/10.1061/(asce)he.1943-5584.0000433)

Vicente-Serrano, S. M., Quiring, S. M., Peña-Gallardo, M., Yuan, S., & Domínguez-Castro, F. (2020). A review of environmental droughts: Increased risk under global warming? *Earth-Science Reviews*, 201(August 2019), 102953. <https://doi.org/10.1016/j.earscirev.2019.102953>

Wan, W., Zhao, J., Li, H. Y., Mishra, A., Hejazi, M., Lu, H., et al. (2018). A Holistic View of Water Management Impacts on Future Droughts: A Global Multimodel Analysis. *Journal of Geophysical Research: Atmospheres*, 123(11), 5947–5972. <https://doi.org/10.1029/2017JD027825>

- Wanders, N., Wada, Y., & Van Lanen, H. A. J. (2015). Global hydrological droughts in the 21st century under a changing hydrological regime. *Earth System Dynamics*, 6(1), 1–15. <https://doi.org/10.5194/esd-6-1-2015>
- Wang, F., Wang, Z., Yang, H., Di, D., Zhao, Y., Liang, Q., & Hussain, Z. (2020). Comprehensive evaluation of hydrological drought and its relationships with meteorological drought in the Yellow River basin, China. *Journal of Hydrology*, 584(June 2019), 124751. <https://doi.org/10.1016/j.jhydrol.2020.124751>
- Wilhite, D., & Pulwarty, R. S. (2017). *Drought and water crises: integrating science, management, and policy*. (CRC Press, Ed.).
- Wilhite, D. A., & Glantz, M. H. (1985). Understanding the drought phenomenon: The role of definitions. *Water International* 10:3, 10, 111–120. <https://doi.org/10.4324/9780429301735-2>
- Wu, J., Chen, X., Yao, H., Gao, L., Chen, Y., & Liu, M. (2017). Non-linear relationship of hydrological drought responding to meteorological drought and impact of a large reservoir. *Journal of Hydrology*, 551, 495–507. <https://doi.org/10.1016/j.jhydrol.2017.06.029>
- Wu, J., Chen, X., Yao, H., Liu, Z., & Zhang, D. (2018). Hydrological Drought Instantaneous Propagation Speed Based on the Variable Motion Relationship of Speed-Time Process. *Water Resources Research*, 54(11), 9549–9565. <https://doi.org/10.1029/2018WR023120>
- Wu, J., Yao, H., Chen, X., Wang, G., Bai, X., & Zhang, D. (2022). A framework for assessing compound drought events from a drought propagation perspective. *Journal of Hydrology*, 604(November 2021), 127228. <https://doi.org/10.1016/j.jhydrol.2021.127228>
- Yun, X., Tang, Q., Wang, J., Li, J., Li, Y., & Bao, H. (2023). Reservoir operation affects propagation from meteorological to hydrological extremes in the Lancang-Mekong River Basin. *Science of the Total Environment*, 896(July), 165297. <https://doi.org/10.1016/j.scitotenv.2023.165297>
- Zhang, X., Hao, Z., Singh, V. P., Zhang, Y., Feng, S., Xu, Y., & Hao, F. (2022). Drought propagation under global warming: Characteristics, approaches, processes, and controlling factors. *Science of the Total Environment*, 838(19), 156021. <https://doi.org/10.1016/j.scitotenv.2022.156021>
- Zhu, Y., Wang, W., Singh, V. P., & Liu, Y. (2016). Combined use of meteorological drought indices at multi-time scales for improving hydrological drought detection. *Science of the Total Environment*, 571(1), 1058–1068. <https://doi.org/10.1016/j.scitotenv.2016.07.096>
- Zink, M., Samaniego, L., Kumar, R., Thober, S., Mai, J., Schafer, D., & Marx, A. (2016). The German drought monitor. *Environmental Research Letters*, 11(7). <https://doi.org/10.1088/1748-9326/11/7/074002>

ANEXO

Anexo A: Material suplementario artículo

A continuación, se presentan las tablas y figuras que forman parte del material suplementario del artículo que se enviará a la revista científica.

Table S.1: Description of parameters and their range of values used to calibrate the SUMMA hydrological model.

Parameter	Description	Units	Calibration range	
			Min	Max
Ksoil	Hydraulic conductivity of soil	m/s	1E-7	1E-4
θsat	Porosity	-	0.30	0.60
CritSoilTranspire	Critical Volume of liquid water content when transpiration is limited	-	0.00	1.00
vGnn	Van Genuchten "n" parameter	-	1.00	2.00
vGnα	Van Genuchten "alpha" parameter	1/m	-1.00	-0.01
aquiferBaseflowExp	Baseflow exponent	-	1.00	10.00
aquiferBaseflowRate	Baseflow rate when aquifer storage is equal to Aquifer Scale Factor	m/s	1E-9	0.10
summerLAI	Maximum leaf area index at the peak of the growing season	m ² / m ²	0.01	10.00
qSurfScale	Scaling factor in the surface runoff parameterization	-	1.00	100.00
heightCanopyBottom	Height of bottom of the vegetation canopy above ground surface	m	0.00	5.00
heightCanopyTop	Height of top of the vegetation canopy above ground surface	m	0.05	100.00
windReductionParam	Canopy wind reduction parameter	-	0.00	1.00
routingGammaScale	Scale parameter in Gamma distribution used for sub-grid routing	s	360	86400
routingGammaShape	Shape parameter in Gamma distribution used for sub-grid routing	-	1.00	5.00
Fcapil	Capillary retention as a fraction of the total pore volume	-	0.01	0.10
αDecayRate	Albedo decay rate	s	1E+6	5E+6
αmax	Maximum snow albedo for a single spectral band	-	0.70	0.95
Kmacropore	Saturated hydraulic conductivity for macropores	m/s	1E-7	1E-1
Ksnow	Hydraulic conductivity of snow	m/s	0.005	0.05
tempCritRain	Critical temperature where precipitation is rain	K	272.16	274.16
refInterceptCapSnow	Reference canopy interception capacity per unit leaf area (snow)	kg/m ²	1.00	10.00
refInterceptCapRain	Canopy interception capacity per unit leaf area (rain)	kg/m ²	0.01	1.00
mwexp	Exponent for meltwater flow	-	1.00	5.00
throughfallScaleSnow	Scaling factor for throughfall (snow)	-	0.10	0.90
throughfallScaleRain	Scaling factor for throughfall (rain)	-	0.10	0.90
wettingFrontSuction	Green-Ampt wetting front suction	m	0.10	1.50

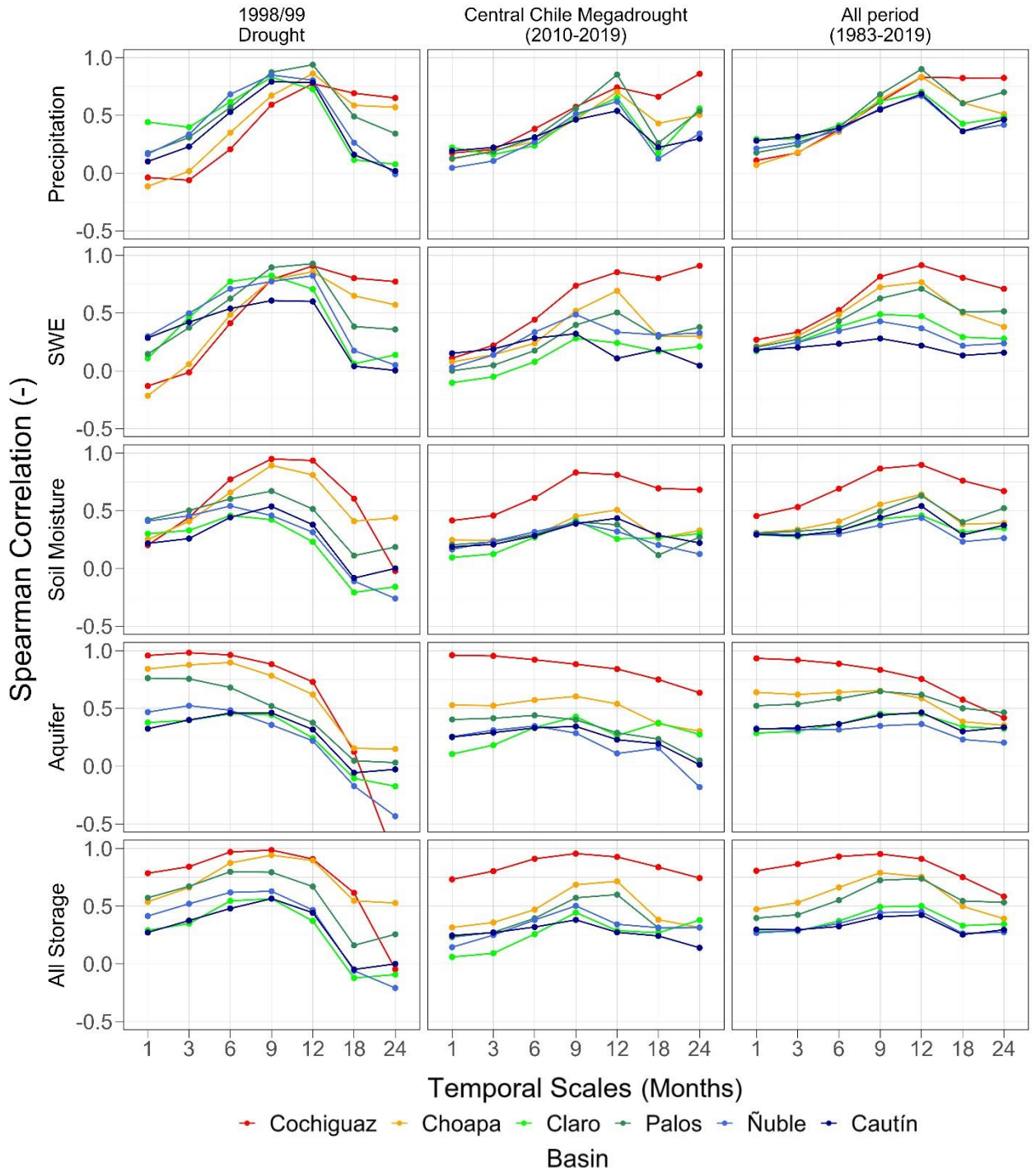


Figure S.1: Spearman rank correlation coefficients between SSI-1 and temporally aggregated/averaged catchment-scale explanatory variables (rows) for three different periods: the October/1998-September/1999 drought event, (b) the central Chile megadrought (April/2010-March/2019), and (c) the entire analysis period (April/1983 - March/2020).

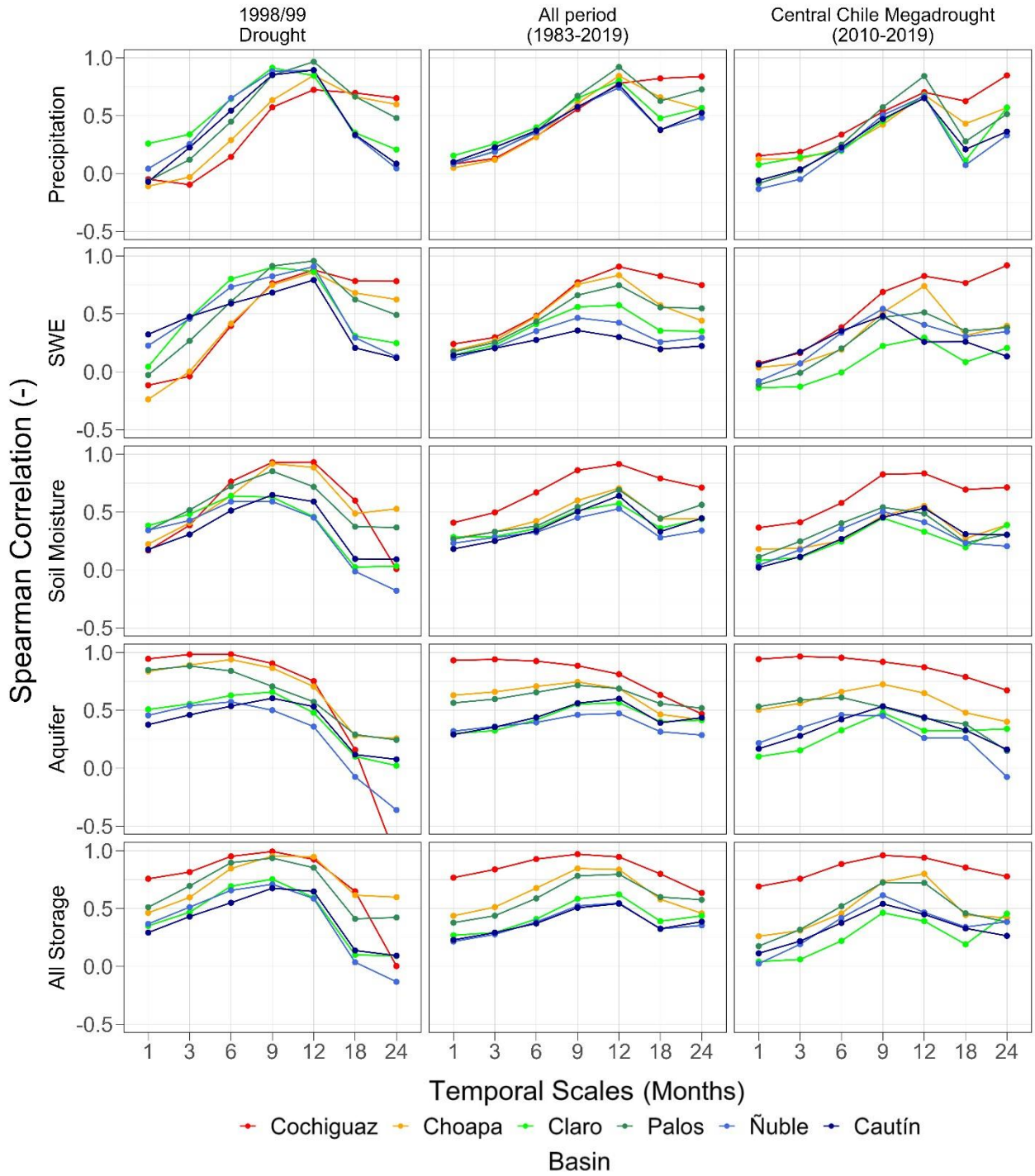


Figure S.2: Spearman rank correlation coefficients between SSI-3 and temporally aggregated/averaged catchment-scale explanatory variables (rows) for three different periods: the October/1998-September/1999 drought event, (b) the central Chile megadrought (April/2010-March/2019), and (c) the entire analysis period (April/1983 - March/2020).

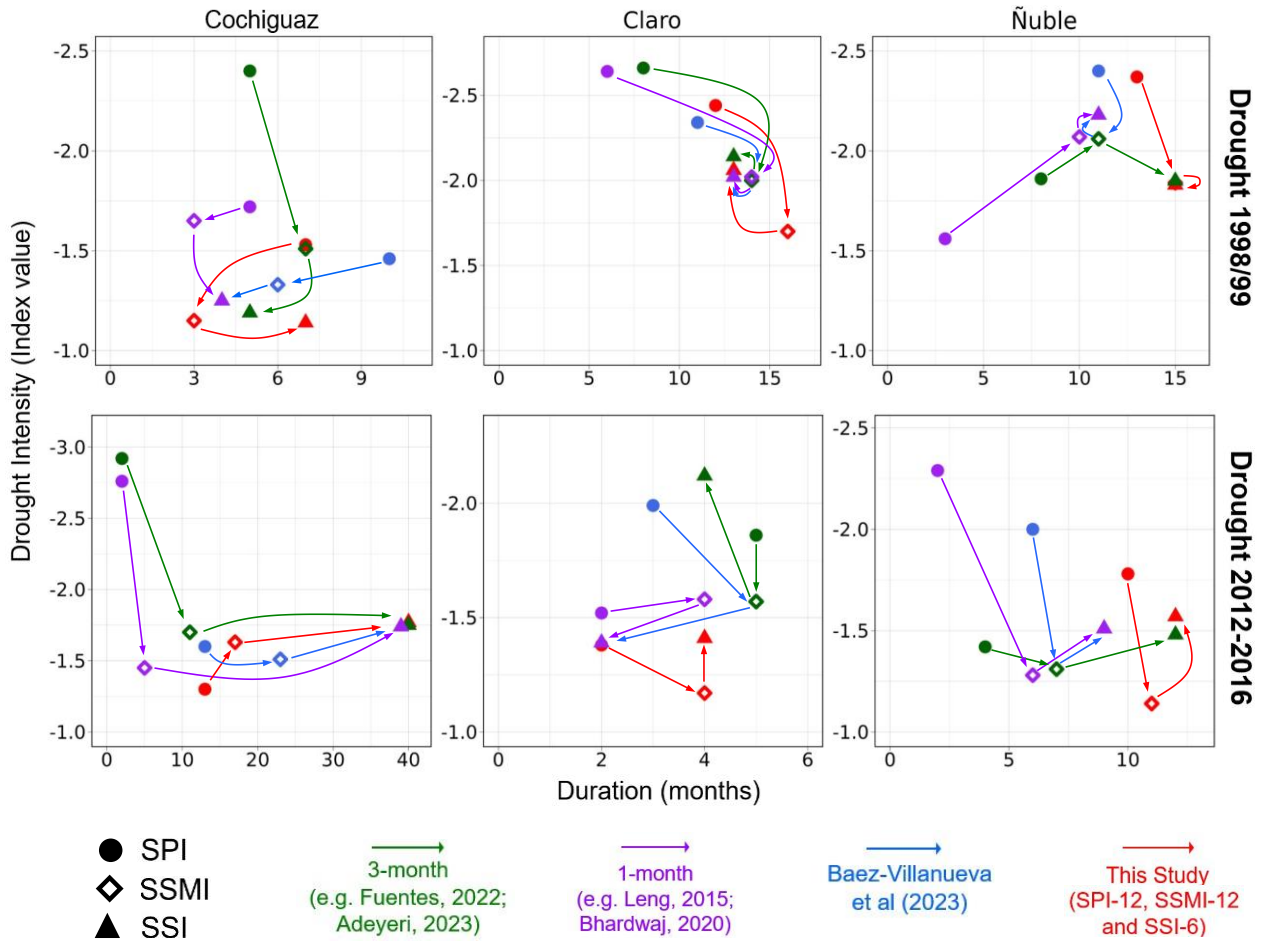


Figure S.3: Propagation from meteorological (circles) to agricultural (diamonds) and hydrological (triangles) droughts for two selected events (1998/99 and 2016/17, displayed in different rows) and three basins with different hydrological regimes: (a) Cochiguaz (snowmelt-driven, left), (b) Claro (rainfall-driven, center) and Ñuble (mixed regime, right). The x-axis shows the duration in months, and the y-axis displays the intensity. The colors indicate trajectories obtained with time scales recommended by different studies (see text for details).

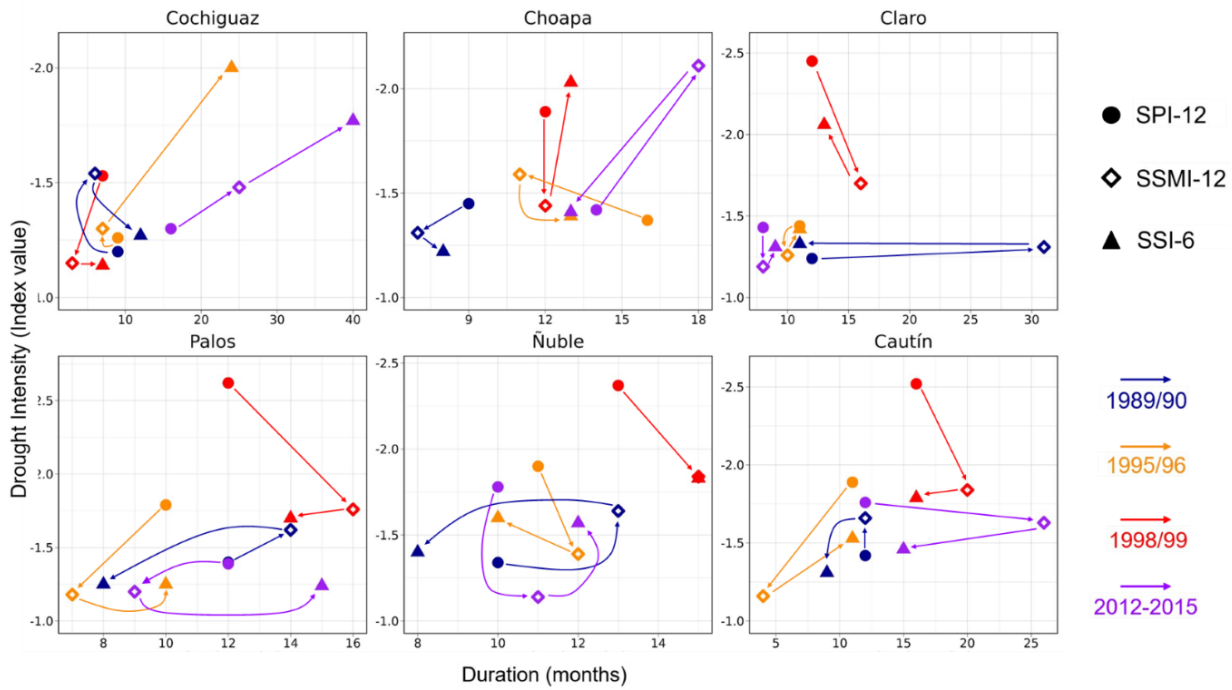


Figure S.4: Propagation from meteorological (circles) to agricultural (diamonds) and hydrological (triangles) droughts for four selected events (1989/1990, 1995/96, 1998/99 and 2012/15, shown with different colors) for the six case study basins. The x-axis shows the duration in months, and the y-axis displays the intensity. The time scales used to compute the standardized indices were selected based on exploratory correlation analysis (see main manuscript for details).